A Review on Direct Power Control of Pulsewidth Modulation Converters

Shuo Yan, *Member, IEEE*, Yongheng Yang, *Senior Member, IEEE*, S. Y. Hui, *Fellow, IEEE*, and Frede Blaabjerg, *Fellow, IEEE*

***Abstract*—Starting from the principle of instantaneous power theory, this article explores various direct power control (DPC) strategies for three-phase two-level pulsewidth modulation (PWM) converters. After summarizing the fundamental power formula of PWM rectifiers, this article studies the operating principle of the conventional table-based approach and its related improvements. It further looks into the advanced counterparts employing space vector modulation and different nonlinear control strategies. The emphasis is put on the prevailing predictive DPC. Besides, the voltage-sensorless and robust DPC methods based on the virtual flux concept and the state observer or estimator are investigated. Critical issues, including the sample delay, constant switching frequency, duty cycle optimization, objective function, and unbalanced operation are examined.**

***Index Terms*—Direct power control (DPC), instantaneous power theory, predictive control, pulsewidth modulation (PWM) converters, space vector modulation (SVM).**

NOMENCLATURE

Variables and Symbols

$\mathbf{S}$	Instantaneous complex power.
$\mathbf{T}$	Extended instantaneous complex power.
$\mathbf{e}$	Supply voltage space vector.
$\mathbf{i}$	Converter current space vector.
$\mathbf{v}$	Converter voltage space vector.
ψ	Virtual flux space vector.
p, q	Instantaneous active and reactive power.
Δp, Δq	Instantaneous active and reactive power increment.
P, Q	Average value of active and reactive power.
e_{abc}	Supply voltages in the three-phase stationary frame.
e_α, e_β	Supply voltages in the two-phase stationary frame.
E	Magnitude of the supply voltage.
E_d, E_q	Supply voltages in the two-phase rotating frame.
θ_E	Initial phase angle of the supply voltage.
θ_I	Initial phase angle of the converter current.
θ	Phase angle of the supply voltage.
v_{abc}	Converter voltages in the three-phase stationary frame.
v_α, v_β	Converter voltages in the two-phase stationary frame.
V_d, V_q	Converter voltages in the two-phase rotating frame.
i_{abc}	Converter currents in the three-phase stationary frame.
i_α, i_β	Converter currents in the two-phase stationary frame.
I	Magnitude of the converter current.
I_d, I_q	Converter currents in the two-phase rotating frame.
$V_{\rm dc}$	DC voltage.
L, r	Inductance and resistance of the L filter.
L_s, r_s	Inductance and resistance of the power supply.
ω	Fundamental angular speed of supply voltage.
r^p, r^q	Active and reactive power rate.
t_s	Sampling frequency.
n	Number of samples.
i	Number of prediction steps.
m	Sector number.
Re()	Real part of space vectors.
Im()	Imaginary part of space vectors.

Superscripts

$+$, $-$	Positive and negative sequence.
ref	Reference value.
ext	Extended p-q theory.
$*$	Conjugate value.
^	Estimated value.
$'$	One-quarter cycle delay.

Subscripts

a, b, c	Three-phase stationary frame.
α, β	Two-phase stationary frame.
d, q	Two-phase rotating frame.
k	Number of converter voltage space vectors.

List of Abbreviations

PWM	Pulsewidth modulation.
VOC	Voltage-oriented control.
DPC	Direct power control.
SVM	Space vector modulation.

Manuscript received November 15, 2020; revised February 22, 2021; accepted March 29, 2021. Date of publication April 2, 2021; date of current version June 30, 2021. This work was supported by the Startup Fund of RMIT University under Grant RI-00101-021. Recommended for publication by Associate Editor A. M. Trzynadlowski. *(Corresponding author: Shuo Yan.)*

Shuo Yan is with the School of Engineering, RMIT University, Melbourne, VIC 3000, Australia (e-mail: shuo.yan@rmit.edu.au).

Yongheng Yang is with the Department of Electrical Engineering, Zhejiang University, Hangzhou 310027, China (e-mail: yang_yh@zju.edu.cn).

S. Y. Hui is with the School of Electrical and Electronic Engineering, Nanyang Technological University, Singapore 639798, Singapore, and also with the Department of Electrical and Electronic Engineering, Imperial College London, London SW7 2BX, U.K. (e-mail: ron.hui@ntu.edu.sg).

Frede Blaabjerg is with the Department of Energy Technology, Aalborg University, 9220 Aalborg, Demark (e-mail: fbl@et.aau.dk).

Color versions of one or more figures in this article are available at https://doi.org/10.1109/TPEL.2021.3070548.

Digital Object Identifier 10.1109/TPEL.2021.3070548

PLL	Phase-locked loop.
DTC	Direct torque control.
VF	Virtual flux.
PI	Proportional–integral.
MPC	Model predictive control.
SMC	Sliding mode control.
BS	Backstepping.
P-DPC	Predictive direct power control.
FCS	Finite control set.
TB	Table-based.
ORS	Output regulation subspace.
GVM	Grid voltage modulated.
OSS	Optimal switching sequence.
FOLPF	First-order low-pass filter.
NF	Notch filter.
SOGI	Second-order general integrator.
QSG	Quadrature sequence generator.
LO	Luenberger observer.
KF	Kalman filter.
MRAS	Model-reference adaptive system.
SMO	Sliding mode observer.
P, I, D, R	Proportional, integral, differential, resonant.
SRF	Synchronous rotating frame.
CCF	Complex-coefficient filter.
ISC	Instantaneous symmetrical component.
VSI	Voltage source inverter.
ROVI	Reduced-order vector integrator.
THD	Total harmonic distortion.
DFIG	Doubly fed induction generator.
ST	Supertwisting.
NPC	Neutral point clamped.
APF	Active power filter.

I. Introduction

THE pulsewidth modulation (PWM) converter has a wide range of applications in power processing due to its merits of regeneration abilities, regulated dc voltage, low current distortion, and high power factor [1], [2]. To utilize the full capacity of PWM converters, various control strategies have been proposed over the past decades. They can mainly be categorized into voltage-oriented control (VOC) and direct power control (DPC). In general, VOC employs inner current loops to calculate the voltage reference and uses space vector modulation (SVM) to synthesize switching pulses. In the literature, different linear and nonlinear control techniques have been developed in the synchronous, stationary, or natural frame [3]. Nevertheless, the overall performance of VOC highly depends on the quality of the inner current loop [4] and the bandwidth of the phase-locked loop (PLL) for synchronization [5]. In contrast, DPC aims to regulate PWM converters by using the active and reactive power as control variables directly. It originates from the direct torque control (DTC) and utilizes the instantaneous power theory as the mathematical framework. The pros and cons of VOC and DPC strategies are summarized in Table I.

TABLE I
Pros and Cons of VOC and DPC Strategies

CONTROL	ADVANTAGES	DISADVANTAGES
VOC	• Constant switching frequency • Advanced PWM strategies are applicable • Low-price sensors and processors • Robust to parameter variations	• Use of coordinate transformation • Active and reactive decoupling is required • Complex control structure • Controller tuning
DPC	• No PWM blocks • No inner current loops • No coordinate transformation • Decoupled active and reactive power control • Simple control structure • No controller tuning is required	• Variable switching frequency • Large interfacing inductor is required • High sampling frequency is required • Fast sensors and processors are required

The first DPC was proposed in 1991, in which a switching table was established to control the active and reactive power of PWM rectifiers based on the sign of the desired power change and the grid-voltage angular position [6]. Since then, different tables have been proposed based on either the grid-voltage or the virtual flux (VF) concept. However, limited improvements are conceived since the use of hysteresis comparators for power regulation leads to a variable switching frequency and requires a high sampling frequency for good control performance. To tackle these problems, DPC is implemented with proportional–integral (PI) regulators and the SVM scheme to directly compensate for the active and reactive power [7]. Such a DPC-SVM is further established to compensate for voltage dips and harmonics in nonideal conditions [8]. In recent decades, tremendous efforts have been made to enhance the capability of DPC by utilizing advanced nonlinear controllers. Prevailing implementations include model predictive control (MPC) [9], sliding mode control (SMC) [10], backstepping (BS) control [11], boundary control [12], and fuzzy logic [13]. In particular, the combined use of DPC and MPC creates an important group of predictive DPC (P-DPC) solutions. These techniques have been extensively investigated in terms of control performance, design complexity, and digital implementation. In addition to the well-known finite-control-set P-DPC (FCS-P-DPC) and deadbeat P-DPC, advanced techniques based on the state observers and/or estimators were developed to explore the voltage-sensorless and robust P-DPC [14]. Improvements aiming to operate DPCs in nonideal supply conditions have been broadly discussed in the literature as well [15]–[17]. A summary of various DPCs is provided in Table II. Although there are many DPC solutions, a general benchmarking is missing to assist the design and control of high-performance PWM converters.

This article reviews the state-of-the-art DPCs for three-phase two-level PWM converters. In Section II, the classic instantaneous power theory is briefly explained and its implications on different DPCs are addressed. Section III studies the principle of the table-based DPC (TB-DPC) and related improvements. Section IV looks into the DPC-SVM. In Section V, various P-DPCs are categorized into the FCS-P-DPC and the deadbeat P-DPC. Section VI continues the discussion of

TABLE II
SUMMARY OF VARIOUS DPC

TYPES OF DIRECT POWER CONTROLS		REFERENCES	ANALYZING METHOD	PROS	CONS
Table-based direct power controls*	Voltage-based	[6]. [20-23], [25]	Simplified power rate (12)	Removal of pulse-width modulation, phase-locked loop, and current loops#	Non-constant switching frequency; high sampling frequency; high values of inductance
		[24], [30]	Complete power rate (9)		
		[33], [34]	Output regulation subspace	Improved vector selection considering the inductor voltage drop	Increased design complexity
	Virtual-flux-based	[26], [28], [32]	Pure integrator for virtual flux/power estimation	Improved dynamics; resilience to unbalanced and distorted conditions; low total harmonic distortion	Sensitive to DC drift and initial bias; reliance on the inductance value of filters
		[31]	Output regulation subspace	Improved vector selection; consideration of power limits	Pure integrator; increased design complexity
Direct power control with space vector modulation		[7], [37]	Virtual-flux-based power calculation	Constant switching frequency; direct compensation of power error with proportional-integral controllers;	Tuning effort; coupled active and reactive power control
		[8], [38]	Voltage-based power calculation		
		[35]	Voltage-based output regulation subspace	Refined reference vector	Increased computational burden
Predictive direct power control	Finite-control-set predictive direct power control	[9], [39], [40], [56], [66], [67]	Single-vector estimation	Simple control design; the guarantee of global optimal vectors	High power ripple; high sampling frequency
		[24], [30], [34], [41-45], [54], [57], [63], [64]	Two-vector estimation	Improved control performance with duty cycle optimization	High computational burden; duty cycle out of zero to one
		[27], [46-53], [55], [65]	Three-vector estimation		
	Deadbeat predictive direct power control	[32], [58-62]	Inversed power model	Closed-form voltage reference; arbitrary voltage vector	Sensitivity to parameter changes; use of pulse-width modulation
Direct power control with other nonlinear controls	Sliding mode control	[10], [15]	—	Lower sensitivity to supply voltage unbalances and distortions	Chattering issues;
	Backstepping control	[11], [16]	—	Systematic and recursive design; high stability; robust to uncertainties	Complex stability analysis
	Fuzzy logic	[13], [65]	—	Adapt to nonlinearity; easy implementation	Slow response; increased complexity for better accuracy
Voltage-sensorless direct power control	Switching-model-based	[25]	Switching circuit model	Removal of voltage sensors;	High sensitivity;
	Integrator-based	[26], [28]	Pure integrators	Smooth power estimation	Sensitive to dc drift and initial bias;
	Filter-based	[29], [62], [82], [83]	First-order low-pass filters; band-pass filter; Notch filters, Second-order general integrator	Elimination of DC offset and initial bias	Magnitude and phase error in virtual flux; sensitive to frequency variation
	Observer-based	[14], [98-103]	Luenberger observers; sliding mode observers; extended observers;	Robust to parameter mismatches	Tuning of observer parameters; stability issues; convergence speed
Direct power control with parameter estimation		[47]	Ohm's theory	Robustness to parameter mismatches; simplicity	Assumption of unity power factor; invalid for no-load operation; sensitive to frequency variation
		[67]	Constant voltage magnitude	Fast convergence	Sensitive to disturbances
		[104]	Continuity of line currents and DC voltage	Good accuracy	Complexity; slow response due to iteration
		[105], [106]	Least-square evaluation	Real-time estimation	High computational burden
Direct power control for unbalanced operations	Ripple terms calculation	[15-17], [61], [107], [121-122]	Voltage/current sequence separation	Flexible compensation target;	Requirement of sequence separation and phase-locked loops
	Extended power theory	[30], [42], [43], [60], [110], [123], [124]	Extended *p-q* theory	Simple control design; low current distortion	Single compensation target;

* Items in bold style are primary types of direct power controls.
\# Underlined pros and cons are common in one primary type of direct power control.

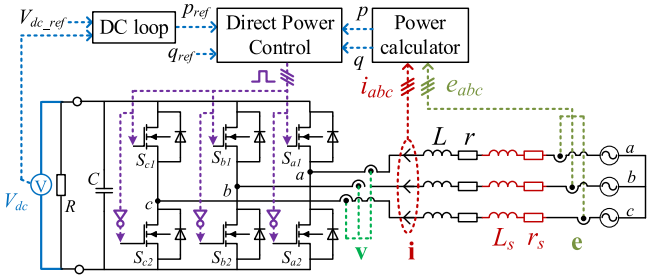

Fig. 1. General schematic of a three-phase two-level PWM rectifier with DPC, where L and r are the inductance and resistance of the L filter; L_s and r_s are the inductance and resistance of the supply; C is the capacitance of the dc capacitor; r is the load resistance.

DPC with other nonlinear control schemes. Section VII inspects the voltage-sensorless and robust DPC with state observers and/or estimators. Section VIII studies the implementation of DPCs under nonideal supply conditions. In Section IX, the performance of typical DPC strategies is compared. Section X discusses applications of DPC in other power electronics systems. Finally, this article is concluded in Section XI.

II. Instantaneous Power Theory

Instantaneous power theory is the mathematical framework of various DPCs. Among different concepts, the classic version (also known as "*p-q* theory") proposed in [18] and generalized in [19] is the standard option. The *p-q* theory defines the physical feature of instantaneous active and reactive power in a three-phase system. Moreover, it provides insights into how the power flows from a source to a load or circulates between phases in a three-phase system. In this section, based on the instantaneous power theory, the important formulas of a three-phase rectifier are summarized. Fig. 1 shows the general schematic and control structure.

A. P-Q *Theory*

The complex power of a three-phase system can be calculated as the dot product of the voltage vector and the conjugate of the current vector as

$$\mathbf{S} = \frac{3}{2}\left(\mathbf{e}\cdot\mathbf{i}^*\right) \tag{1}$$

where e is the space vector of the supply voltage, $\mathbf{i}$ is the space vector of the rectifier current, and "$*$" stands for the conjugate of a complex vector.

The real and imaginary parts of (1) are further defined as the instantaneous active and reactive power, respectively

$$\begin{cases} p = \frac{3}{2}\mathrm{Re}\left(\mathbf{e}\cdot\mathbf{i}^*\right) \\ q = \frac{3}{2}\mathrm{Im}\left(\mathbf{e}\cdot\mathbf{i}^*\right). \end{cases} \tag{2}$$

B. *Power Formula of PWM Rectifiers*

The instantaneous power model of PWM rectifiers is essential for the development of a DPC. According to Fig. 1 and based on Kirchhoff's voltage law (KVL), the voltage balance equation of the circuit is written as

$$\mathbf{e} = r\cdot\mathbf{i} + L\frac{d\mathbf{i}}{dt} + \mathbf{v} \tag{3}$$

where $\mathbf{v}$ is the space vector of the rectifier voltage, and r and L are the resistance and inductance of the inductive filter.

Assuming an ideal source, the supply voltage vector is expressed as

$$\mathbf{e} = Ee^{j\omega t+\theta_E} \tag{4}$$

where E is the magnitude of the supply voltage vector, ω is the fundamental angular speed, and θ_E is the initial phase angle.

Based on the finite switching states, the rectifier has in total eight voltage vectors, consisting of two zero vectors ($\mathbf{v_0}$ and $\mathbf{v_7}$) and six nonzero vectors ($\mathbf{v_1}$, $\mathbf{v_2}$, $\mathbf{v_3}$, $\mathbf{v_4}$, $\mathbf{v_5}$, and $\mathbf{v_6}$). The six nonzero vectors can be denoted in a general way as

$$\mathbf{v}_k = \frac{2}{3}V_{\mathrm{dc}}e^{j\frac{\pi}{3}(k-1)} \tag{5}$$

where $k = (0, 1, 2, 3, \ldots, 7)$ is the number of the vector denoted in Fig. 2 and V_{dc} is the dc voltage of the rectifier. Nonzero vectors separate the voltage space into six sectors, upon which the angular position of the supply voltage or VF is determined.

From (3) and (4), the derivatives of the supply voltage and the rectifier current are written as

$$\frac{d\mathbf{i}}{dt} = \frac{1}{L}\left(\mathbf{e}-\mathbf{v}-r\mathbf{i}\right) \tag{6}$$

$$\frac{d\mathbf{e}}{dt} = j\omega\mathbf{e}. \tag{7}$$

The total derivative of (1) defines the dynamic feature of the instantaneous complex power as

$$\frac{d\mathbf{S}}{dt} = \frac{3}{2L}\left(E^2-\mathbf{e}\cdot\mathbf{v}^*\right) - \frac{1}{L}\left(r-j\omega L\right)\cdot\mathbf{S}. \tag{8}$$

From (8), the instantaneous power rate of active and reactive power is obtained as

$$\begin{cases} \frac{dp}{dt} = \frac{3}{2L}E^2 - \frac{V_{dc}E}{L}\cos\left(\omega t+\theta_E-\frac{\pi}{3}(k-1)\right) - \frac{r}{L}p-\omega q \\ \frac{dq}{dt} = -\frac{V_{dc}E}{L}\sin\left(\omega t+\theta_E-\frac{\pi}{3}(k-1)\right) - \frac{r}{L}q+\omega p. \end{cases} \tag{9}$$

Equation (9) is important in DPC since it mathematically defines the impact of eight voltage vectors on the rate of active/reactive power with respect to the angular position of the

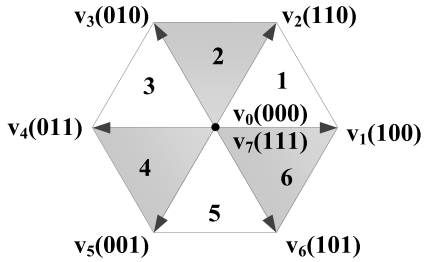

Fig. 2. Voltage space and rectifier voltage vectors. [Note: m= 1, 2, 3, …, 6 is used to indicate the sector number in this article]. .

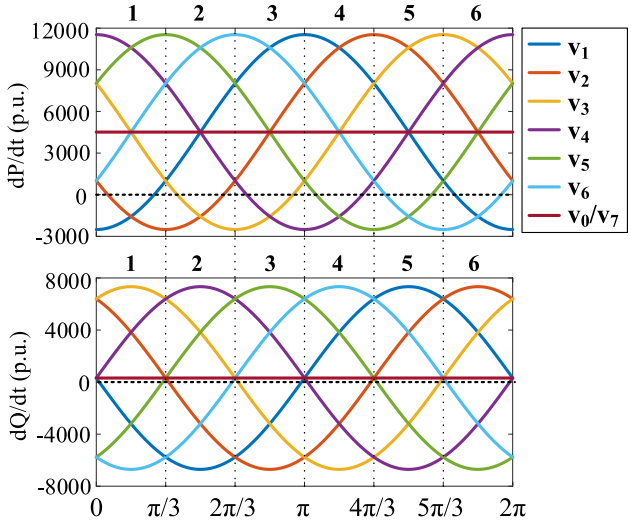

Fig. 3. Example of active/reactive power rate based on (9) in per-unit system. (Parameters in the equation are $E = 120$ V (rms), $V_{\rm dc} = 300$ V, $r = 0.4\ \Omega$, $L = 8$ mH, $\omega = 314$ rad/s, $p = 1000$ W, and $q = 0$ Var.)

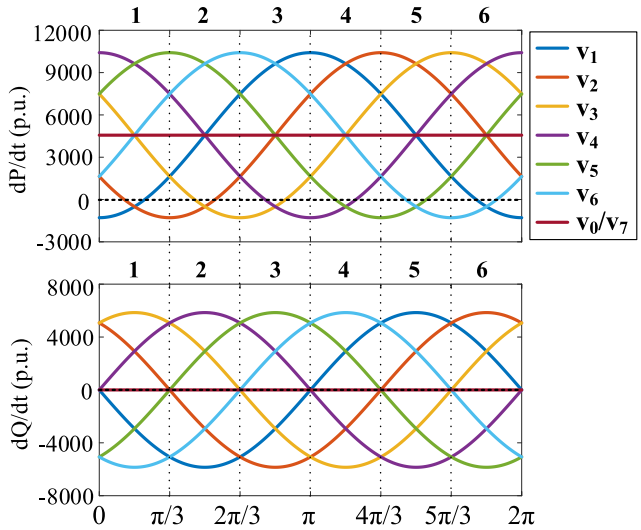

Fig. 4. Example of active/reactive power rate based on (11) in per-unit system. (Parameters in the equation are $E = 120$ V (RMS), $V_{\rm dc} = 300$ V, $r = 0.4\ \Omega$, $L = 8$ mH, $\omega = 314$ rad/s, $p = 1000$ W, $q = 0$ Var.).

supply voltage. In early works on DPC, the derivative of the supply voltage is not considered by assuming an ideal source voltage. Therefore, with negligible inductor resistance, the power rate is readily calculated by multiplying the supply voltage and the current derivative. Hence, (8) and (9) are simplified into (10) and (11), respectively

$$\frac{d\mathbf{S}}{dt} = \frac{3}{2L}\left(E^2 - \mathbf{e}\cdot\mathbf{v}^*\right) \tag{10}$$

$$\begin{cases} \frac{dp}{dt} = \frac{3}{2L}E^2 - \frac{V_{\rm dc}E}{L}\cos\left(\omega t + \theta_E - \frac{\pi}{3}(k-1)\right) \\ \frac{dq}{dt} = -\frac{V_{\rm dc}E}{L}\sin\left(\omega t + \theta_E - \frac{\pi}{3}(k-1)\right). \end{cases} \tag{11}$$

It is a common practice to plot (9) or (11) with each of the eight voltage vectors so that the sign of the power rate with respect to the angular position of the supply voltage can be determined to facilitate the selection of suitable voltage vectors for power control. An example is given in Figs. 3 and 4 based on (9) and (11), respectively. The red-solid straight lines in Figs. 3 and 4 indicate the dc offset of active/reactive power rate. By comparing Figs. 3 and 4, it can be found that ignoring the inductor resistance and the source voltage dynamics leads to the horizontal shift of the active/reactive power rate. Therefore, control logic established based on (11) could be inaccurate, especially at the instant when the power rate is crossing zero. Further simplification of (11) assumes that the initial phase angle of the source voltage is zero (i.e., $\theta_E = 0°$). As a result, a proportional relationship between the power rate and decoupled rectifier voltages is obtained in the two-phase synchronous framework as

$$\begin{cases} \frac{dp}{dt} \propto \frac{3}{2}E - V_d \\ \frac{dq}{dt} \propto V_q \end{cases} \tag{12}$$

where V_d and V_q are the decoupled rectifier voltages in the synchronous framework and are calculated as

$$\begin{cases} V_d = V_{\rm dc}\cos\left(-\frac{\pi}{3}(k-1)\right) \\ V_q = V_{\rm dc}\sin\left(-\frac{\pi}{3}(k-1)\right). \end{cases}$$

III. Table-Based DPC

This section summarizes the TB-DPCs using the supply voltage or VF for vector selection. The essential procedure of establishing a switching table is discussed in detail. Moreover, related improvements are explored.

A. Fundamentals of TB-DPCs

The first TB-DPC was introduced in 1991 [6]. Since then, many improved switching tables have been proposed. These TB-DPCs are different in the table establishment. Early works of TB-DPC adopt the simplified version of the power rate given in (11) or (12) to calculate the sign of the power rate [6], [20]–[23], while refined works utilize the full expression in (9) for more accurate analysis [24].

The establishment of an offline switching table is critical in developing a TB-DPC. The sign of the active and reactive power rate induced by each rectifier voltage vector is inspected so that vectors giving the desired sign in every sector can be selected to form a switching table. Using the digitalized power error as the input, hysteresis comparators are implemented to determine the expected sign of the power rate. In practice, the optimum switching state is selected from the switching table based on the angular position of the source voltage [25] or the VF [26], with the angular position of the selected rectifier voltage applied in a few cases [27]. The typical structure of a TB-DPC is shown in Fig. 5.

The hysteresis band of the comparators has a significant impact on the power regulation and the switching frequency. A smaller bandwidth results in lower power errors but higher switching frequency. Another well-known issue of using hysteresis comparators is the nonconstant switching frequency, which complicates the design of filters and cooling devices. A simple method is proposed in [23]. The hysteresis band of

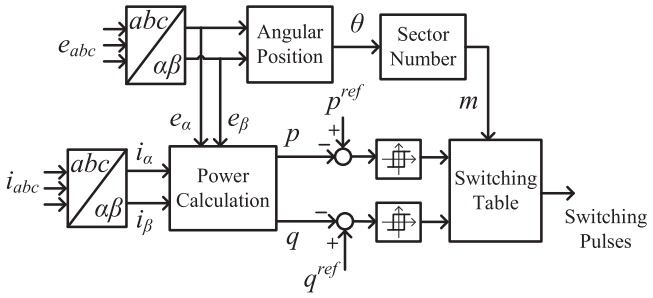

Fig. 5. Typical control structure of a TB-DPC.

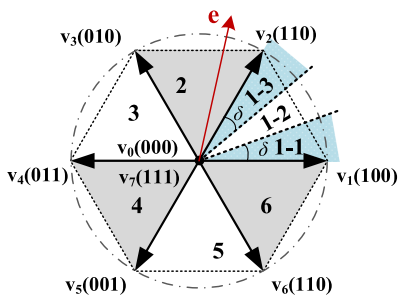

Fig. 6. Arbitrary sector division in an improved table-based DPC method [32].

the comparators is dynamically adjusted with respect to the switching frequency. This approach prevents the unnecessary short switching pulses but fails to achieve the genuine consistent switching frequency.

B. Virtual Flux

The VF concept has a wide range of applications in the electrical motor control. It was originally introduced to improve the performance of voltage-sensorless DPCs. As compared with the voltage-based counterpart, the VF-based DPC can improve the current waveform in nonideal grids and achieve a lower sampling frequency and simpler voltage/power estimations. Besides, it avoids sharp errors of the estimated value at the switching instant.

A comprehensive design of the VF-based DPC is conducted in [28]. The VF vector is defined as the integration of the source voltage

$$\psi = \int \mathbf{e} dt. \tag{13}$$

The derivative of the VF vector results in a new expression of the supply voltage as

$$\mathbf{e} = \frac{d}{dt}(\psi) = \frac{d\psi}{dt} e^{j\omega t} + j\omega \cdot \psi. \tag{14}$$

By assuming an ideal supply voltage, the derivative of the VF's amplitude in (14) can be ignored to simplify the analysis. Therefore, the supply voltage becomes

$$\mathbf{e} = j\omega \cdot \psi. \tag{15}$$

However, this simplification reduces the accuracy of the VF estimation during the startup or sudden voltage changes [29].

Applying the *p-q* theory, the instantaneous active and reactive power based on the VF is derived as

$$\begin{cases} p = \frac{3}{2}\omega \mathrm{Re}\left(j\psi \cdot \mathbf{i}^*\right) \\ q = \frac{3}{2}\omega \mathrm{Im}\left(j\psi \cdot \mathbf{i}^*\right). \end{cases} \tag{16}$$

To design the switching table, the rate of the instantaneous active and reactive power can further be derived as

$$\begin{cases} \frac{dp}{dt} = \frac{3}{2}\omega \mathrm{Re}\left(-\omega\psi \cdot \mathbf{i}^* + \frac{1}{L}\left(\omega|\psi|^2 - j\psi \cdot \mathbf{v}^*\right)\right) \\ \frac{dq}{dt} = \frac{3}{2}\omega \mathrm{Im}\left(-\omega\psi \cdot \mathbf{i}^* - \frac{j\psi \cdot \mathbf{v}}{L}\right). \end{cases} \tag{17}$$

Based on (17), similar plots of the active and reactive rate as in Fig. 3 can be obtained. Following the same design principle as the TB-DPC, VF-based TB-DPC can be developed [26]. Since the VF is broadly applied to derive the voltage-sensorless DPC, the integral method plays an important role in the performance of the VF-based TB-DPC. This aspect will be addressed in Section VII-A.

C. Improvements of the TB-DPC

The switching table in [25] is regarded as a benchmark, to which other switching tables are compared. It is established based on two simple rules: 1) rectifier voltage vectors closer to **e** increase active power, while zero vectors and/or vectors immediately further from **e** decrease active power, and 2) converter vectors leading **e** decrease reactive power, while those lagging **e** increase reactive power. However, this pioneering switching table does not guarantee good power regulation at all intervals. Vectors selected to increase active power and decrease reactive power give false control commands due to the wrong sign of the reactive power rate, thus resulting in significant power ripples and current distortion.

In [24], a general switching table is proposed. The same table is introduced in [30] based on the extended power definition in order to remove the double-fundamental frequency power oscillation of PWM rectifiers in unbalanced conditions. From this general table, another three improved tables can be obtained as in [20]–[22]. The table in [20] replaces the unsuitable row of increasing active power and decreasing reactive power in [25] to reduce the power ripple and current distortion. Bouafia *et al.* [21] make the same change and further replaced zero vectors with active vectors for increasing both active and reactive power. Eloy-Garcia and Alves [22] replace the vectors for increasing and decreasing active power while increasing reactive power. However, these switching tables show a minor difference in the control outcome [31]. Although another three tables can be derived based on different combinations of redundant vectors in [24], they are more of interest in the theoretical study but barely show much performance improvement in practice. In [32], further table improvements are achieved by quantitatively analyzing the impact of voltage vectors on the power rate over one sector. To restrain the power ripple, voltage vectors inducing moderate power change are used in the vicinity of the sector boundaries. Therefore, each sector is further divided into three subsectors having δ, $(60^\circ - 2\delta)$, and δ phase angle, as shown in Fig. 6. Based on this sector division, the 12 sector divisions in [21] and [25] are a special case when δ is equal to 30°.

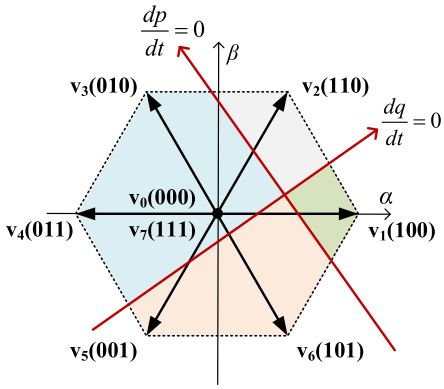

Fig. 7. Example of ORS analysis.

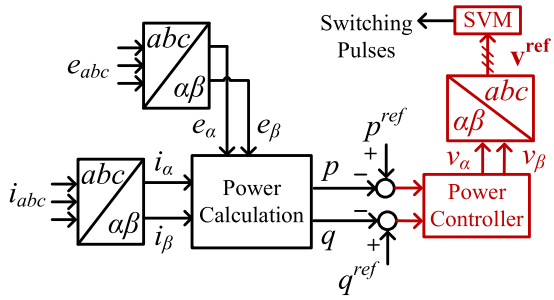

Fig. 8. Typical structure of DPC with SVM.

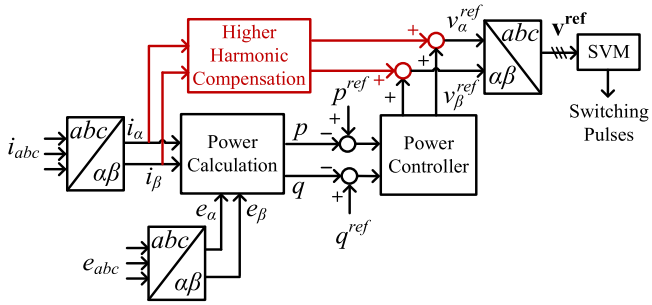

Fig. 9. Structure of the improved DPC with SVM [8].

An underlying assumption of these heuristic switching tables is that the origin of the power rate plane is the same as the origin of the voltage vectors plane by neglecting the voltage drop across the inductor. This assumption results in an inaccurate selection of optimum vectors, especially in the vicinity of sector boundaries. To refine the vector selection, output regulation subspaces (ORS) have been applied [31], [33]–[35]. An example of ORS analysis is shown in Fig. 7. In [33], the ORS modifies the vector selection by rotating the grid vector for a precalculated angle before selecting the rectifier vector to compensate for the voltage drop over the inductor. The angles are calculated to guarantee that the approximate ORS creates the same partition of the subscribed circle as the original ORS so that the zones indicating different combinations of the power rate signs are better determined. Based on similar ORS analysis, Vazquez *et al.* [35] propose a vector reference as the composition of an equivalent vector (the vector pointing from the origin of the voltage vectors plane to the origin of the power rate plane) and a proportion of the source voltage vector and its conjugate. In fact, this ORS-based DPC belongs to the DPC-SVC to be discussed in the next section due to the use of SVM or PWM in synthesizing the reference. In [31], the ORS is applied together with the VF concept to enforce a "voltage-to-power" transformation, by which the circle indicating the inverter voltage limit is converted into another circle defining the power limit. The impact of the inductor voltage drop on the vector selection is addressed by moving the origin of the power rate plane from the terminal of the source voltage vector to the terminal of the vector as the sum of source voltage and the inductor voltage.

Due to the dc offset of the active power rate function (see the upper plot of Fig. 3), the crossover angle of the active power rate takes place inside each sector. The exact value of the crossover angle depends on the real-time value of the dc voltage and the source voltage. If the boosting ratio of the dc voltage is not well designed, the selected vector may reverse the power regulation. To solve this problem, a dynamic switching table is proposed [36]. The dc voltage and supply voltage are fed back to calculate the crossover phase angle and update the switching table dynamically. Apparently, this dynamic table could work appropriately only if the sampling frequency and computational speed are high enough to ensure the real-time establishment of switching tables.

IV. DPC With SVM

The variable switching frequency resulting from hysteresis comparators is a major drawback of conventional TB-DPCs. To overcome this problem, SVM is implemented to generate the voltage reference. Different from the TB-DPC, the DPC-SVM calculates the average voltage reference via linear regulators with active and reactive power as control variables instead of selecting a vector from a switching table. A general control structure of the classic DPC-SVM is shown in Fig. 8. The SVM is also applied to deadbeat P-DPCs to modulate the closed-form voltage reference calculated according to the inverse predictive power model. This category of P-DPC with SVM will be discussed in Section V-B.

The classic DPC-SVM proposed in [7] contains two PI controllers to calculate the stationary voltage reference using the instantaneous active and reactive power errors as control variables. This method was established using the simplified power model that neglects the supply voltage dynamics in the VF-based framework. Besides, the coupling effect of the *d*-*q* rectifier voltage on the rectifier power is not well addressed. In [37], the active filtering feature is added to PWM rectifiers by modifying the classic DPC-SVM. Two high-pass filters are implemented to isolate the harmonic active and reactive power. The sum of the positive-sequence power and harmonic power is used as the input of the PI-based DPC-SVM similar to [7].

An improved DPC-SVM is introduced in [8] to operate the PWM converter in unbalanced and distorted conditions. The structure of this improved DPC-SVM is shown in Fig. 9. As a part of the power calculation, the voltage dip compensation is

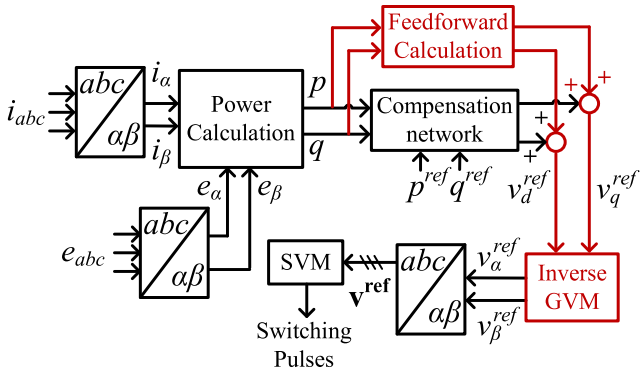

Fig. 10. Structure of the GVM-DPC [38].

achieved by two voltage estimators consisting of a notch filter (NF) and a low-pass filter to isolate the positive- and the negative-sequence supply voltage. The harmonic compensator is in the form of an integrator with a finite dc gain tuned for specific harmonics. Since the controller is deployed in the stationary frame, the park transformation in targeted harmonic frequencies is necessary for the compensation purpose. This implementation results in a high computational burden due to the use of multiple transformation blocks.

Recent work on the DPC-SVM improves the classic DPC-SVM by making use of the power rate model in (9) [38]. The so-called grid voltage modulated direct power control (GVM-DPC) utilizes the intrinsic Clarke transformation formed by the dot product of the grid voltage and the converter voltage in the α-β frame (also called inverse GVM). In other words, the trigonometric terms of the α-β grid voltage are used to form a Clarke transformation matrix to obtain the converter voltage in the *d*-*q* frame. This leads to decoupled active and reactive power control using PI regulators and feedforward terms to obtain the voltage reference. Fig. 10 shows the structure of the GVM-DPC. Although it is convenient to use the stationary grid voltage to enforce the Clarke transformation, the proposed method could be ineffective if the grid voltage contains harmonics and/or negative-sequence components.

V. Predictive Direct Power Control

In the recent decade, MPC has been become a popular technique for power converters due to its simplicity, flexibility, and the convenience of adding control constraints. The combined use of MPC and the instantaneous power theory forms a new family of DPC, known as P-DPC. As compared with the TB-DPC, the P-DPC guarantees the optimal vector selection based on the principle of power ripple minimization.

The FCS-P-DPC and the deadbeat P-DPC are two main streams of P-DPCs. Based on the finite switching state model of PWM converters, FCS-P-DPC uses a single vector or a concatenated vectors' sequence to regulate the instantaneous power. Deadbeat P-DPC uses the inverse predictive model to calculate the voltage reference that nullifies the instantaneous power error at each time step. This section summarizes the key elements of the two types of P-DPCs. Besides, implementation issues including the control delay, the objective function, and

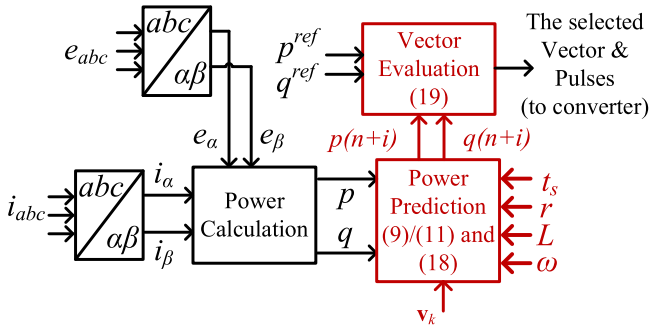

Fig. 11. Structure of a single-vector approach.

A. Finite-Control-Set P-DPC

FCS-P-DPC evaluates the eight switching states of power converters and selects one or several vectors in one control cycle to achieve the optimized power regulation. Based on the power rate function in (9) or (11), the converter power in the next time step is predicted as

$$\begin{cases} p\left(n+i\right) = p\left(n\right) + \Delta p \\ q\left(n+i\right) = q\left(n\right) + \Delta q \end{cases} \tag{18}$$

where $p(n)$ and $q(n)$ are, respectively, the active/reactive power measured at the *n*th cycle, Δp and Δq are the predicted power increase in one or more time-step, respectively, and *i* defines the number of the prediction horizon.

The incremental terms on the right-hand side of (18) vary in response to the number of vectors applied. It predicts the amount of power change induced by the selected vector(s) within a fixed time horizon. In one-vector approaches, the increment is the product of the time step and the power rate of the selected vector. In multivector approaches, the incremental terms are the sum of power changes induced by all selected vectors.

To evaluate rectifier vectors, an objective function is imposed to predict the power error so that the vector or the sequence of vectors giving the minimum power error can be determined. The objective function is common in the form of the square sum as in (19). Although the absolute sum of the power error is used in some works, it is more convenient to apply the following equation in further mathematical operations:

$$\text{obj} = \left(p^{\text{ref}} - p\left(n+i\right)\right)^2 + \left(q^{\text{ref}} - q\left(n+i\right)\right)^2 \tag{19}$$

where p^{ref} and q^{ref} are the active and reactive power references, respectively.

Equations (18) and (19) are rudimentary in FCS-P-DPCs as they carry out the key steps of power prediction and power error evaluation.

1) Single-Vector Approaches: In [9], the conventional FCS-P-DPC using a single vector is introduced. A two-step predictive model is developed to evaluate the power variation induced by voltage vectors so that the one giving the minimum power error is selected. Although the P-DPC using a single vector is intuitive to implement, a high sampling frequency is necessary in order to achieve a good reference tracking performance. The structure of the single-vector FCS-P-DPC is shown in Fig. 11.

In [39], a preselection scheme is introduced to reduce the switching loss by prohibiting the switching operation of the

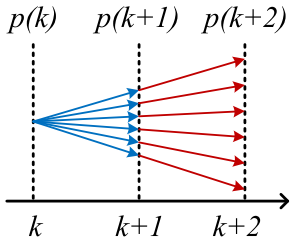

Fig. 12. Vector selection criterion in [40].

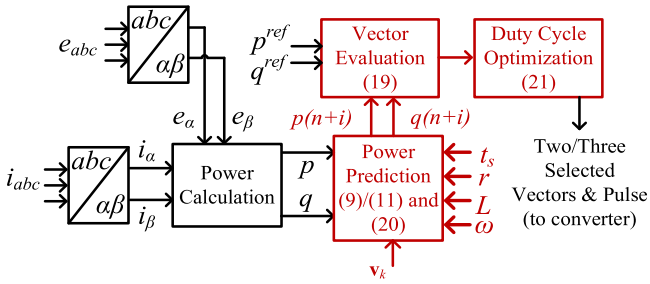

Fig. 13. Structure of model predictive approach using two or three vectors.

are examined by the objective function to determine the optimum one in each control period. The proposed approach requires a two-step prediction of both rectifier current and power, thus exhibiting an increased control complexity.

A simplified two-step prediction is developed to reduce the switching frequency in [40]. The objective function calculates the total power error in the first and the second time step. Instead of examining all 49 (7×7) combinations, the proposed approach evaluates the same vector in the first and the second time step. Therefore, the number of the vector sequences to be examined is reduced from 49 to 7. The selection criterion is shown in Fig. 12. Although the computational burden is significantly reduced, the use of the same vector in two time steps could not ensure the global minimization of power errors.

2) Two-Vector Approaches: Applying one vector during one control period is limited in exerting the full potential of the FCS-P-DPC. Therefore, two vectors' approaches have been extensively investigated. In two vectors' approaches, the one-step power prediction is written as

$$\begin{cases} p(n+1) = p(n) + [r_1^p t_1 - r_2^p (t_s - t_1)] \\ q(n+1) = q(n) + [r_1^q t_1 - r_2^q (t_s - t_1)] \end{cases} \tag{20}$$

with r_1^p, r_2^p, r_1^q, and r_2^q the active and reactive power rates of the first and the second voltage vector, respectively, t_1 the application time of the first voltage vector, and t_s the sampling period.

Based on the first derivative test, the cost function is differentiated toward the time interval of the first active vector as in (21). The solution calculates the optimized duty cycle giving the minimum value of the objective function. The general structure of two-vector FCS-P-DPC is shown in Fig. 13.

$$\frac{\mathbf{d}\text{obj}}{\mathbf{d}t_1} = 0. \tag{21}$$

A simple two-vector P-DPC using one active vector and one zero vector is proposed in [24], [34], and [41]–[43]. The active vector can be selected online using the power error evaluation [42] or from a predefined table [43]. The application interval of the chosen vectors is optimized toward the minimization of the objective function. A fraction of the control period is allocated for an active vector and the remaining time for a zero vector.

The use of zero vectors to fill up the control cycle is intended to enforce the moderate power change. However, this idea is feasible only if zero vectors have no significant impact on active and reactive power. As shown in Fig. 3, zero vectors have a negligible impact on reactive power but a noticeable influence on active power. To address this problem, a different vector sequence is proposed in [44] and [45]. Instead of using strictly an active plus a zero vector, the vector sequence is relaxed to one active plus either a zero or an active vector for better steady-state performance. To find the optimal vector pair, Bozorgi *et al.* [44] propose a repetitive evaluation of 12 pairs (six pairs consisting of an active plus a zero vector and six pairs comprised of two consecutive active vectors) in one control period. The duty cycle of the first active vector is calculated by the Mamdani fuzzy logic, and the Lyapunov function is used to exclude pairs violating the stability criterion. As a result, the proposed evaluation method has high complexity due to the use of the fuzzy logic modulator and the online stability examination. A simplified two-step vector selection is proposed in [45] based on the low-complexity evaluation originally proposed for motor control. The first vector is chosen as the one nearest to a reference vector, while the second vector is chosen geometrically based on the region (that defines the minimum tracking error among two adjacent active vectors and two zero vectors) toward which the reference vector points. This approach avoids the repetitive calculation of the optimal duty cycle and the evaluation of the cost function, thus exhibiting a quick selection feature.

3) Multiple-Vector Approaches: More sophisticated multi-vector P-DPC methods using three vectors are originally proposed in [46] and [47] and further improved in the vector selection approach [27], [48]–[51] and the arbitrary vector formation [52], [53].

Similar to the two-vector approach, the three-vector approach predicts the rectifier power with a sequence of three vectors and uses the objective function for power evaluation. Therefore, the one-step power prediction is written as

$$\begin{cases} p(n+1) = p(n) + [r_1^p t_1 + r_2^p t_2 + r_0^p (t_s - t_1 - t_2)] \\ q(n+1) = q(n) + [r_1^q t_1 + r_2^q t_2 + r_0^q (t_s - t_1 - t_2)] \end{cases} \tag{22}$$

where r_1^p, r_2^p and r_1^q, r_2^q are, respectively, the active and reactive power rate of the two active vectors; $r_0^p$and r_0^q are, respectively, the active and reactive power rate of the zero vectors; t_1 and t_2 are, respectively, the application time of the two active vectors.

Based on the first derivative test, (22) is differentiated toward the time interval of the two active vectors, as given in (23). The solution calculates the optimal duty cycles giving the minimum value of the objective function. The structure of the three-vector

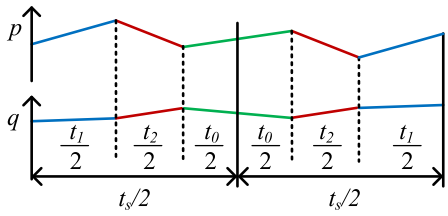

Fig. 14. Example of "3+3" vectors' sequence.

approach is similar to the two-vector approach shown in Fig. 13.

$$\begin{cases} \frac{\partial \text{obj}}{\partial t_1} = 0 \\ \frac{\partial \text{obj}}{\partial t_2} = 0. \end{cases} \tag{23}$$

The classic method adopts two symmetrical concatenated switching patterns using three vectors, known as "3+3 vectors' sequence" [46], [47]. An example is shown in Fig. 14. Using the angular position of the grid vector, the approach selects two active vectors and one zero vector according to the rule of the minimum communication number. Such a vector selection logic is similar to the design rule of table-based schemes, resulting in limited performance improvements in steady state. To refine the power vector selection, Vazquez *et al.* [50] introduce the predictive optimal switching sequence (OSS). The OSS calculates the optimized duty cycle of all 12 vectors' sequences and evaluates the corresponding power error to select the optimal sequence. Although the global optimal sequence is ensured without calculating the angular position of the grid voltage, the high computational burden increases the control complexity significantly. To simplify the vector selection, Song *et al.* [51] propose a strategy to establish the vector sequence without using sector information and the angular position of the source voltage. The proposed strategy adopts fixed voltage vectors and uses the sign of the optimized duty cycle and their combinations to determine the actual vectors and their optimized duty cycle. Besides, a duty cycle reconstruction scheme is proposed to enable the symmetrical distribution of selected vectors and circumvents the faulty values of the duty cycle (i.e., duty cycle smaller than zero or larger than one).

In fact, using the first derivative test to calculate the optimal duty cycle could result in a value exceeding the range from 0 to 1. The intuitive approach of limiting the value saturation causes immediate control failures, such as the sudden power surge. In [27], [48], and [49], the issue of a duty cycle smaller than zero ("$D < 0$") is inspected. Results show that in the ending part of even sectors in 12-sector cases (equivalent to the ending part of all sectors for 6-sector cases), selected vectors result in a positive reactive power rate. The minimization of the cost function leads to a negative duration time of the secondary active vector. To address this problem, the secondary active vector is replaced by another active vector producing a negative reactive power rate in the ending part of odd sectors. In [54], the issue of duty cycle larger than one ("$D > 1$") is studied. Results show that the selection of appropriate vectors depends on not only the sign but also the absolute value of the induced power rate. If a voltage vector inducing an insufficient power rate, an increase in the duty cycle can be observed, which further causes current spikes and power surge. To address this issue, a new table containing an additional precalculated interval in every sector is developed to eradicate the "$D > 1$" case and its associated power quality issues.

Recent developments of the multivector approach interpret the vector sequence from a different perspective [52], [53]. The so-called arbitrary vector formation separates the converter vector optimization into "phase" (or direction) and "length" (or amplitude) optimization. Two adjacent active vectors are first selected by evaluating all six combinations. Based on the principle of objective function minimization, their duty cycle is optimized to ensure that the synthesized vector has the same angular position as the reference vector. The second step repeats the duty cycle optimization by using the synthesized vector and a zero vector to optimize the length. Although better performance is obtained, the algorithm has a high computational burden due to the repetitive evaluation and optimization of the objective function. To handle this issue, a novel multivector approach using the parallelogram geometry for duty cycle optimization is proposed in [55]. A generic equation of converter vectors is established to simplify the vector selection and the duty cycle optimization, without using the objective function and the first derivative test.

To reduce the evaluation complexity, a low-complex evaluation is proposed to facilitate the vector evaluation in [56]. The negative conjugate of complex power in the synchronous frame is introduced as the new control variable to indicate the length and direction of the ideal converter vector so that only one prediction is required to select the converter vector nearest to the ideal vector. It is proved that the objective function of the low-complex P-DPC is the same as that of the FCS-P-DPCs. The low-complex approach is further extended to the multivector approach in [57]. In addition to the quick vector selection, the duty cycle optimization is much simplified.

B. Deadbeat P-DPC

Deadbeat P-DPC is another mainstream of P-DPCs. In this approach, the optimum space-vector voltage is calculated to eliminate the power error. SVM is adopted to synthesize the optimal vector in every control cycle. The deadbeat P-DPC improves over the table-based approach in terms of constant switching frequency, less harmonic distortion, lower computational requirement, and faster tracking speed. As compared with FCS-P-DPC, the deadbeat P-DPC avoids the repetitive evaluation of the objective function for vector selection and duty cycle optimization.

In deadbeat P-DPCs, the complex-power rate is rewritten based on the first-order forward Euler method as

$$\frac{\mathbf{S}(n+1) - \mathbf{S}(n)}{t_s} = \frac{d\mathbf{S}(n)}{dt}. \tag{24}$$

By replacing the next-step power with the reference value (i.e., $\mathbf{S}(n+1) = \mathbf{S}^{\text{ref}}$), (24) gives a set of linear equations. Its solution offers the closed-form reference of the converter voltage, which leads to the zero power error at the end of the next time step. This reference is modulated by SVM to create switching pulses. The structure of the deadbeat P-DPC is shown in Fig. 15.

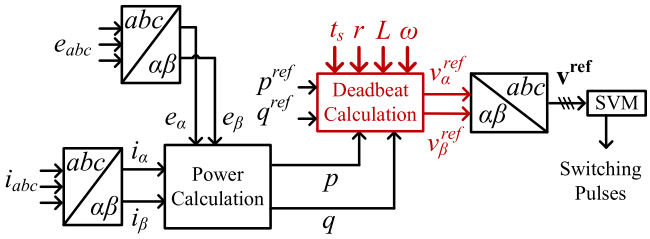

Fig. 15. Structure of the deadbeat predictive DPC.

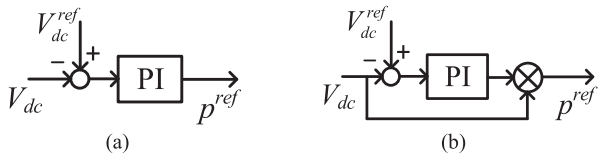

Fig. 16. DC voltage loop. (a) PI control. (b) PI control with the feed-forward dc voltage.

In [58], the optimum rectifier voltage vector is developed in the α-β frame in balanced conditions. A simplified equation of the optimum space vector is introduced in [59] by neglecting the inductor resistance and the supply-voltage variation. The optimum voltage reference is computed in both the α-β and d-q frames. Using the same deadbeat principle and control structure, Zhang and Qu [60] replace the original reactive power with the extended reactive power to improve the performance of the deadbeat DPC in unbalanced grids. Although the derived reference equation using this theoretical framework is more complex than the one using the conventional power definition, the proposed method is capable of obtaining sinusoidal rectifier current and eliminating the double fundamental frequency power ripple in unbalanced grids. In [61], additional oscillation terms are added to the constant power reference contained in the equivalent voltage reference to restrain the dc voltage oscillations under unbalanced grids. However, the stabilization of the dc voltage is achieved at the expense of oscillating active/reactive power.

In [32], the calculation of the reference voltage is introduced in the stationary frame based on VF. The equation is derived based on the simple deadbeat principle of driving the power error to zero. To compensate for the power error caused by the nonnegligible angular move of source flux at the low sampling frequency, the angle compensation is used to rotate the reference components for a small angle for better control accuracy. Cho and Lee [62] introduce another optimum vector calculation using VF. However, only active power is used as the control variable in deriving the optimum vector equation with the reactive power untreated. Additionally, the method results in high current distortion under unbalanced grids.

C. Implementation Issues of P-DPC

1) Control Delay: In digital implementation, the one-step delay is a common problem of P-DPC. The voltage vector computed at the present nth cycle will not be applied until the next $(n+1)$th cycle, which results in the error of the power prediction. To address this problem, a two-step prediction is commonly adopted. The instantaneous power at the $(n+2)$th cycle is calculated using the predicted grid voltage, converter voltage, and converter current at the $(n+1)$th cycle. The power at the $(n+2)$th is applied in the cost function to generate the control command [40]–[42], [45], [52], [53], [56], [57], [60], [63], [64].

Some latest works on P-DPC consider the one-cycle delay as a type of external disturbance and suggest the use of state observers or disturbance estimators to compensate for the delay. This implementation conceals a new category of P-DPCs aiming to improve the control robustness against system uncertainties and sensitivity, which will be examined in Section VII.

2) Objective Function: Improvements of the conventional objective function in (19) can be found in some studies. In [40], the objective function is modified to address the power error in a two-step prediction. The active/reactive power errors in the first and the second prediction are contained in one objective function. Another two-step objective function is used in [63] to evaluate only the active power, with the purpose to minimize the active power ripple.

The use of square sum in (19) could lead to mutual interference during active and reactive power control. If either active or reactive power has a large variation, the control weight is concentrated on one side. In [64], the objective function is reconfigured to have two weighting factors that can be adjusted in response to the error term of the corresponding active and reactive power. By adding these weighting factors, the mutual interference between active and reactive power in (19) can be minimized. Li *et al.* [65] introduced a similar method in which the fuzzy logic modulator is used to obtain weighting factors based on the absolute active/reactive power error.

In [66], the objective function is further expanded to contain the normalized dc voltage constraints. The constraints of active and reactive power are normalized and weighted to ensure that the control action is allocated evenly among the three control variables. A similar approach using the absolute error of control variables is discussed in [67].

3) Power Reference: In most TB-DPCs and P-DPCs, the active power reference is calculated by a dc voltage controller using a PI regulator [see Fig. 16(a)] while the reactive reference is manually set to zero for unit power factor or other arbitrary values for auxiliary grid services [9], [39], [51], [53], [58], [64]. An improved option [see Fig. 16(b)] is to multiply the PI output and the feed-forward dc voltage to improve the control dynamics [34], [41]–[43], [45], [46], [56], [57], [59]–[61], [63].

These standard implementations of the dc voltage loop are based on the assumption that the active power flow is balanced between the input and output of the PWM converter. However, this may not be valid when the zero vector is applied. To address this problem, Quevedo *et al.* [66] propose a new filtered dc voltage reference and the compatible active reference without using a control loop. The filtered dc voltage reference is calculated to converge to the true voltage reference within a fixed horizon. The active power reference is hence calculated by multiplying the filter dc reference and the rectifier current with the consideration of the power loss on the inductor resistance. This calculation of

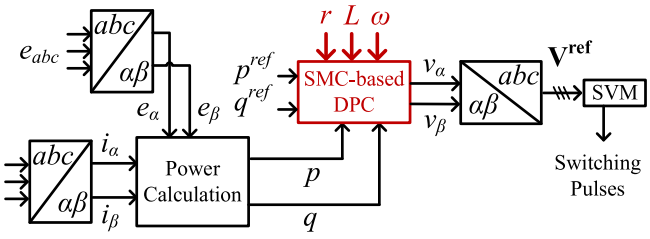

Fig. 17. Structure of the DPC based on SMC.

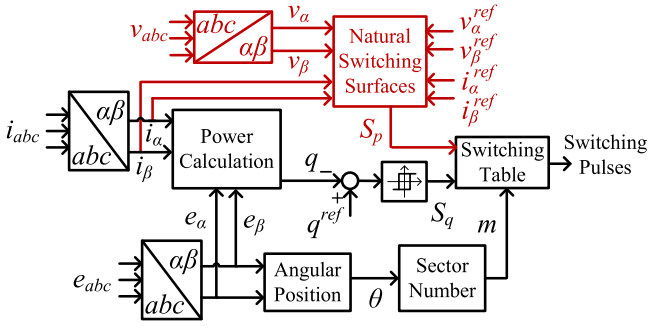

Fig. 18. Structure of the DPC based on natural switching surfaces in [12].

the dynamic reference ensures the coupling of input and output power at all instants.

VI. DPC Employing Other Nonlinear Controls

DPC strategies employing other nonlinear control methods have also been proposed in the literature. Based on the Lyapunov stability principle, SMC is implemented together with the DPC concept to directly calculate the converter's reference voltage in the α-β frame [10], [15]. Fig. 17 shows the typical structure of SMC-based DPC.

A DPC based on a natural switching surface is proposed by using boundary control in [12]. In regulating the active power, the proposed method uses the rectifier voltage rather than the active power as the control variable for the selection of the switching states. As a result, the dynamic performance of the dc voltage control is improved due to the omission of the voltage loop. However, the reactive power control uses the same hysteresis comparator as in classic TB-DPC. Besides, one extra voltage sensor is needed to acquire the rectifier voltage. Fig. 18 shows the control structure.

A BS control technique was applied together with DPC and SVM due to its merits of systematic and recursive design methodology. A BS-DPC strategy is presented in [16] to control the ac/dc converter with a flexible power compensation and good dynamic performance under balanced and unbalanced grid conditions. Another BS-DPC with a second-order dc voltage and active power subsystem and a first-order reactive power subsystem is introduced to address system uncertainties [11]. The structure is similar to the SMC-based DPC in Fig. 17.

In [13], fuzzy logic rules are used to select the best switching state of the converter at each sampling time, with the aim to get rid of the predefined switching table. By using the normalized active/reactive power error as the fuzzy logic variables, the hysteresis comparator is no longer needed, which results in

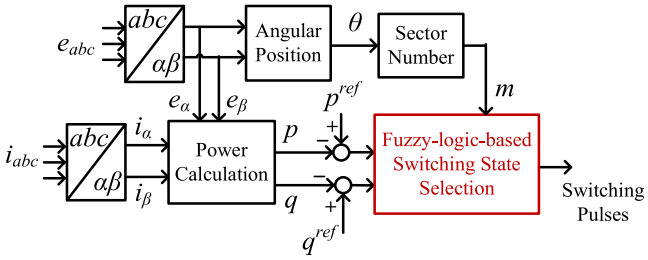

Fig. 19. Structure of the DPC based on fuzzy logic rules [13].

smooth power control. Still, the method is very similar to a TB-DPC using the simplified power rate in (11), although the proposed table is established based on fuzzy logic rules rather than the sign of active/reactive power errors. The general control structure is shown in Fig. 19.

VII. DPC Employing Observers and Estimators

A. Voltage-Sensorless DPCs

Sensorless control has a long history in ac motor drives [68], [69]. Existing voltage-sensorless DPCs are based on the duality with the PWM inverter-fed induction motor where the estimated flux signal is used in the speed-sensorless vector control. In this section, DPCs employing estimators and observers for the voltage-sensorless operation are investigated. Based on different estimation algorithms, voltage-sensorless DPCs are summarized into the filter-based and the observer-based approaches.

1) Filter-Based Approaches: The voltage-sensorless DPC is initially proposed in [25]. Based on the KVL theorem, the grid voltage is estimated by adding the voltage drop on the *L*-filter to the rectifier voltage. Although this model-based approach is easy to implement, the computation of the time derivative of measured currents introduces high noise sensitivity, especially at the instant of switching actions. To prevent the differential calculation, a VF-based voltage-sensorless DPC is suggested [26]. The inherent filtering capability of the pure integrator [see Fig. 20(a)] improves the accuracy of power estimation under unbalanced and distorted grid conditions. However, the pure integrator suffers from the dc offset and initial bias in practical applications. This problem has been extensively studied in the sensorless vector control of ac motors, especially in low-speed operations. A common solution is to replace the pure integrator with the first-order low-pass filter (FOLPF), as shown in Fig. 20(b). However, the FOLPF induces the magnitude and phase errors in the estimated VF [29]. Although these errors can be minimized by setting a low cutoff frequency, the reduction of bandwidth degrades the effectiveness of rejecting the dc offset.

A lot of efforts have been made to improve the VF estimation of FOLPFs. The prevalent approach of adding a feedback term to the transfer function of FOLPFs is introduced in [70], as shown in Fig. 20(c). Three closed-loop integrators are proposed and have been benchmarked with other integrators. The first and the second integrators improve the FOLPF with saturate feedback. Although the accurate VF prediction can be achieved at steady-state conditions, the technique fails to work at transient states. The third integrator enforces the estimated flux vector to lag the

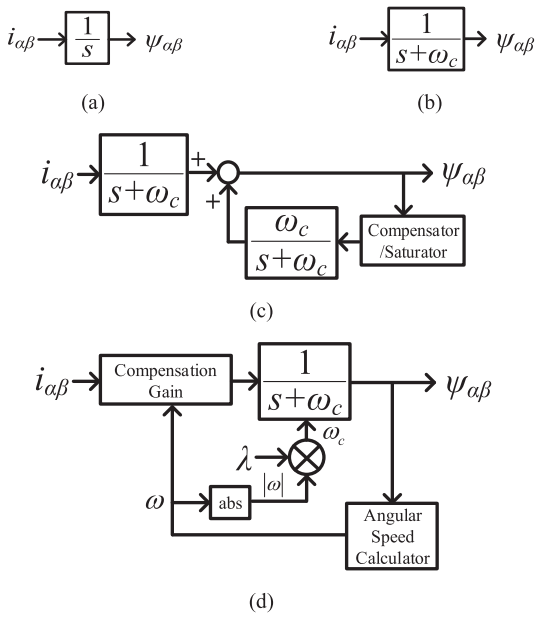

Fig. 20. Integration methods for VF estimation. (a) Pure integrator. (b) FOLPF, in which ωc is the cutoff frequency. (c) Closed-loop FOLPF. (d) Frequency-adaptive FOLPF, in which λ is the design constant and ω is the angular speed of the source voltage.

induced voltage vector for 90° by using a PI regulator to change the amplitude of the VF compensation term in response to the dc offset or the initial value. However, the assumption of absolute orthogonality between the motor flux and the back electromotive force (emf) is invalid when disturbances are present in the source voltage. To deal with the frequency deviation, the programmable FOLPF has been proposed [71]–[74], as shown in Fig. 20(d). The frequency of VF is estimated in each control cycle to adaptively change the cutoff frequency and the compensation gain of the FOLPF. Therefore, an accurate calculation of the flux frequency is critical to the performance of the adaptive FOLPF.

Other filters have also been applied to estimate the VF in some references. Approaches based on band-pass filters are proposed to enhance the freedom of shaping the frequency response [75]–[77]. However, small errors in the amplitude or phase angle of the estimated VF are still found in these methods. In [78], NFs based on the cascaded linear neural networks are proposed to eliminate the dc component in the calculation of the VF. Due to the use of only one bias weight, the neural-network-based NF is simple to implement as compared with the traditional fixed-frequency NF. Several frequency-independent fast algorithms based on high-pass filters were proposed in [79]. However, they are valid when only the fundamental-frequency component is present in the voltage space vector. To improve the estimation accuracy without compensating magnitude and phase angle, several VF calculators based on the second-order general integrator (SOGI) are proposed [80], [81]. Configured as a quadrature signal generator (QSG), the SOGI is inherently frequency-adaptive and is capable of performing sequence separation.

In principle, the above filter-based approaches in the sensorless vector control of ac motors are equally applicable in the voltage-sensorless DPC that requires accurate VF estimations.

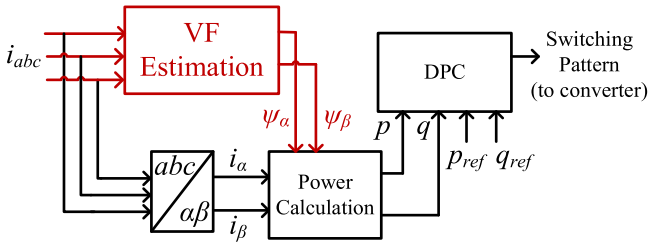

Fig. 21. Structure of a sensorless DPC with VF estimation.

The structure of filter-based VF estimation is shown in Fig. 21. In [29], a fast open-loop FOLPF is introduced to improve the dynamic response of the VF estimation. The magnitude and phase errors are compensated by examining the transfer function of FOLPFs at the operating frequency. The gain and angle shift are utilized to reconstruct the VF. Obviously, the open-loop integrator can improve the dynamics but has immediate stability limitations when the frequency deviation occurs. In [62], a programmable approach similar to that in [71]–[74] is applied to improve the VF estimation of a deadbeat P-DPC. The frequency of the estimated VF is calculated in real time and is fed back to change the compensation gain and the cutoff frequency of FOLPFs. In [82] and [83], VF-based P-DPCs using SOGI are proposed. Due to the small number of works on this topic, there is an interest in inspecting the performance of other filter-based VF estimations in the voltage-sensorless DPC.

2) Observer-Based Approaches: Observer-based approaches have a broad range of applications in the speed/position-sensorless control of ac motors [69], [84]. In these approaches, the error between the plant and observer outputs is usually used as the input signals to the observer. The observer gain is designed to force the error to zero so that the estimated value for the states of interest can converge to their actual value. Popular techniques, including the Luenberger observer (LO), Kalman filter (KF), model-reference adaptive system (MRAS), and sliding mode observer (SMO), have been applied.

The LO is a common technique that uses the full- or reduced-order model to predict the states of interest. It minimizes the error of the measured and the estimated outputs based on a PI or proportional–integral–differential compensator. Despite its simplicity, the LO is limited in rejecting the noise contained in the feedback signal, hence resulting in inaccurate values in the estimated states of interest. To overcome this drawback, approaches using the KF as a statistically optimal observer have been proposed [85]–[88]. For KFs, satisfactory noise rejection is achieved at the expense of a high computational burden. Besides, the process noise parameters are needed for tuning of the observer, which is usually determined by trial and error [89]–[92]. The MRAS is another linear scheme for state estimation. In an MRAS, an adjustable model and a reference model are connected in parallel. The output of the adjustable model is expected to converge to the output of the reference model using a proper adaptation mechanism [93]–[95]. The SMO is a popular nonlinear alternative that uses discontinuous functions of the estimated-measured state error as inputs (usually a sign function). It relies on the nonlinear high-gain feedback to drive estimated states to a hypersurface where the error between the

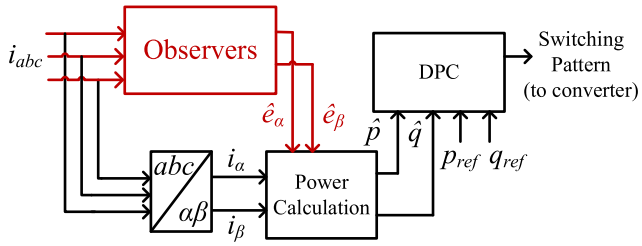

Fig. 22. Structure of a sensorless DPC with observers.

estimated and the actual value is zero. Besides, using the sign of the error to drive the SMO could reduce its sensitivity to many forms of noise [96], [97].

In voltage-sensorless DPC, the use of observers is a recent development to improve the control stability when variations in the source impedance and computational delay are expected. The general structure is shown in Fig. 22. In [98] and [99], a simple LO is used to compensate for the control delay and to eliminate the grid voltage sensors. A similar LO is employed in [100] to predict the complex power term in the voltage reference acquired from a complex-variable instantaneous power model. In order to reduce the total harmonic distortion (THD) in the output current, the proposed approach further implements a fundamental frequency positive sequence detector based on the sliding discrete Fourier transformation in conjunction with a source voltage observer derived from a discrete state-space model.

The SMO is employed to derive a voltage-sensorless DPC in [101]. Based on the constant plus proportional rate search law, the SMO is implemented to estimate the grid voltage in unbalanced grids. The fundamental positive- and negative-sequence components are inherently separated to facilitate the design of an FCS-P-DPC without employing cascaded filters as in [96]. The embedded filtering function of SMO also attenuates the high-frequency chattering and dc offsets. Although the proposed voltage-sensorless P-DPC presents fast dynamic responses and a quick startup capability, parameter mismatches of the source impedance would introduce estimation errors. In [14], a similar SMO is employed to improve the steady-state performance of the deadbeat P-DPC. The complex power contained in the equivalent voltage reference is predicted to compensate for the estimation error caused by mismatched parameters and the one-step delay. The equivalent voltage reference is further calibrated by subtracting the disturbance term estimated by a control function that enforces the error to decay exponentially. Another SMO is developed in [102]. The Sigmoid function with continuous variable boundary thickness is adopted to estimate the source voltage of a VF-based DPC by using the current error as the observer input. The VF is estimated based on the integrator with PI compensator in [70]. The proposed scheme improves the estimation accuracy and dynamic response but requires large efforts to tune the control parameters.

In [103], a discrete extended-state observer is implemented to reduce the impact of varying grid impedance. The observer bandwidth and cutoff frequency are tuned so that the attenuation of system disturbance is guaranteed at any given frequency. However, the stability analysis and the parameter tuning of the observer result in heavy computation.

B. Impedance Estimation of P-DPCs

In P-DPC, the value of the source impedance plays an important role in obtaining an accurate power estimation. For example, in deadbeat P-DPCs, this parameter is directly used to calculate the equivalent voltage reference. Any model uncertainty or parameter mismatch would result in significant performance deterioration.

To address this problem, an online estimation of source impedance has been considered. In [47], a simple online impedance estimator is added to the multivector P-DPC based on the VF concept. Under the assumption of a unity power factor, the impedance is estimated using Ohm's theory by dividing the source voltage magnitude over the inductor current module. Since the inductor current module is used as the denominator, the estimation has to be bypassed in the zero load condition. The method uses the second-order low-pass filter to restrain the high-frequency oscillation in the voltage module, resulting in a slow dynamic response. This implementation further induces stability issues due to the nonzero initial value. An improved technique is discussed in [104]. The method utilizes the continuity of the estimated grid voltage module and the estimated active/reactive power before and after the commutation change. Since the calculation depends on the switching state and the time derivative of the converter current, the estimated inductance contains much noise. In [67], the source impedance is estimated by solving an equation obtained under the assumption of a constant grid voltage magnitude in every two sampling cycles. Apparently, this method is not applicable in nonideal grid conditions. Kwak *et al.* [105] propose a general technique, in which the effect of the model inaccuracy is first studied. The observation from experimental results shows that the underestimated inductance worsens the current distortion, the power error, and the power factor, while the overestimated impedance deteriorates the current distortion but has a negligible effect on the power factor and power errors. An adaptive online identification technique is further proposed to calculate the input inductor parameter in every sampling cycle based on the least-square principle. The rectifier current is predicted using the previous rectifier current and voltage, and it is compared with the present sampling value to establish a least-square error function. The input inductance and resistance of the rectifier are thus determined by minimizing the error function. Another weakening factor least square algorithm is implemented to enforce the online inductance estimation of a deadbeat P-DPC [106]. Although the proposed method is simple to implement, its performance relies on the design of the factor value that affects the convergence rate and the error fluctuation.

VIII. DPC in Nonideal Conditions

A. Power Analysis

1) P-Q Theory: Since voltage imbalance commonly exists in power systems, the DPC has been developed to improve

system reliability and power quality in unbalanced grids. The popular sequence analysis is often applied to denote the voltage and current as the sum of the positive- and negative-sequence components given as

$$\begin{cases} \mathbf{e} = \mathbf{e}^{+} + \mathbf{e}^{-} = E^{+}e^{j\omega t} + E^{-}e^{-j\omega t} \\ \mathbf{i} = \mathbf{i}^{+} + \mathbf{i}^{-} = I^{+}e^{j\omega t} + I^{-}e^{-j\omega t} \end{cases} \tag{25}$$

where E^{+} and E^{-} are the amplitude of the positive- and negative-sequence supply voltage, respectively, and $I^{+}$and I^{-} are the amplitude of the positive- and negative-sequence converter current, respectively.

Due to the existence of negative-sequence components, the power ripple with twice the grid fundamental frequency would appear. It is usually caused by four interactions between:

1) fundamental positive-sequence voltage and fundamental negative-sequence current;
2) fundamental negative-sequence voltage and fundamental positive-sequence current;
3) fundamental positive-sequence voltage and third-harmonic positive-sequence current;
4) fundamental negative-sequence voltage and fundamental negative-sequence third-harmonic current [17].

Since the magnitude value of the fourth component is much smaller than the other three, it is reasonable to assume that the converter current contains I^{+}, I^{-}, and I^{3+}. In some cases [42], [43], the third harmonic current is also ignored to further simplify the power analysis.

The calculation of the oscillating power terms can be carried out in either the α-β or *d-q* framework. Some publications recommend the α-β frame to avoid the use of a PLL and its associated problems [107].

Replacing (25) into (2), the instantaneous power of a three-phase system is obtained as

$$\begin{cases} p = p_0 + p_1 + p_2 \\ q = q_0 + q_1 + q_2 \end{cases} \tag{26}$$

where p_0 and q_0 are the dc components of active and reactive power, respectively, and p_1, p_2, and q_1, q_2 are the double fundamental-frequency components of active and reactive power, respectively. In the α-β frame, these power terms are defined as

$$\begin{pmatrix} p_0 \\ p_1 \\ p_2 \\ q_0 \\ q_1 \\ q_2 \end{pmatrix} = \begin{pmatrix} e_\alpha^{+} & e_\beta^{+} & e_\alpha^{-} & e_\beta^{-} \\ 0 & 0 & e_\alpha^{+} & e_\beta^{+} \\ e_\alpha^{-} & e_\beta^{-} & 0 & 0 \\ e_\beta^{+} & -e_\alpha^{+} & e_\beta^{-} & -e_\alpha^{-} \\ 0 & 0 & e_\beta^{+} & -e_\alpha^{+} \\ e_\beta^{-} & -e_\alpha^{-} & 0 & 0 \end{pmatrix} \begin{pmatrix} i_\alpha^{+} \\ i_\beta^{+} \\ i_\alpha^{-} \\ i_\beta^{-} \end{pmatrix} \tag{27}$$

in which

$$\begin{cases} e_\alpha^{+} = E^{+}\cos\left(\omega t + \theta_E^{+}\right) \\ e_\beta^{+} = E^{+}\sin\left(\omega t + \theta_E^{+}\right) \\ e_\alpha^{-} = E^{-}\cos\left(-\omega t + \theta_E^{-}\right) \\ e_\beta^{-} = E^{-}\sin\left(-\omega t + \theta_E^{-}\right) \end{cases}$$

$$\begin{cases} i_\alpha^{+} = I^{+}\cos\left(\omega t + \theta_I^{+}\right) \\ i_\beta^{+} = I^{+}\sin\left(\omega t + \theta_I^{+}\right) \\ i_\alpha^{-} = I^{-}\cos\left(-\omega t + \theta_I^{-}\right) \\ i_\beta^{-} = I^{-}\sin\left(-\omega t + \theta_I^{-}\right). \end{cases}$$

The extension of (4) leads to the power definition in the *d-q* frame as

$$\begin{cases} p = P_0 + P_{c2}\cos\left(2\omega t\right) + P_{s2}\sin(2\omega t) \\ q = Q_0 + Q_{c2}\cos\left(2\omega t\right) + Q_{s2}\sin(2\omega t) \end{cases} \tag{28}$$

where P_{c2}, P_{s2} and Q_{c2}, Q_{s2} are, respectively active and reactive power ripples oscillating at twice the fundamental frequency. These power terms are defined as

$$\begin{pmatrix} P_0 \\ P_{c2} \\ P_{s2} \\ Q_0 \\ Q_{c2} \\ Q_{s2} \end{pmatrix} = \frac{3}{2}\begin{pmatrix} E_d^{+} & E_q^{+} & E_d^{-} & E_q^{-} \\ E_d^{-} & E_q^{-} & E_d^{+} & E_q^{+} \\ E_q^{-} & -E_d^{-} & -E_q^{+} & E_d^{+} \\ E_q^{+} & -E_d^{+} & E_q^{-} & -E_d^{-} \\ E_q^{-} & -E_d^{-} & E_q^{+} & -E_d^{+} \\ -E_d^{-} & -E_q^{-} & E_d^{+} & E_q^{+} \end{pmatrix} \begin{pmatrix} I_d^{+} \\ I_q^{+} \\ I_d^{-} \\ I_q^{-} \end{pmatrix} \tag{29}$$

in which

$$\begin{cases} E_d^{+} = E^{+}\cos\left(\theta_E^{+}\right) \\ E_q^{+} = E^{+}\sin\left(\theta_E^{+}\right) \\ E_d^{-} = E^{-}\cos\left(\theta_E^{-}\right) \\ E_q^{-} = -E^{-}\sin\left(\theta_E^{-}\right) \end{cases} \tag{30}$$

$$\begin{cases} I_d^{+} = I^{+}\cos\left(\theta_I^{+}\right) \\ I_q^{+} = I^{+}\sin\left(\theta_I^{+}\right) \\ I_d^{-} = I^{-}\cos\left(\theta_I^{-}\right) \\ I_q^{-} = -I^{-}\sin\left(\theta_I^{-}\right). \end{cases} \tag{31}$$

2) Extended P-Q Theory: In 1997, Konastu and Kawabata introduced the "extended *p-q* theory" to address the control issues of active filters in unsymmetrical voltage systems [108]. The new definition of reactive power complies with the commonly agreed concept that the instantaneous reactive power is the sum of the algebraic product of the conjugate of phase current and the quadrature-phase voltage lagging the actual voltage by 90°. Suh and Lipo improved this theory by using complex vectors in the *d-q* frame. The ripple component of instantaneous reactive power is more clearly defined to have the same mathematic expressions as the ripples of active power [109]. This makes it possible to nullify the oscillating components of instantaneous active/reactive power simultaneously, hence achieving a simple control structure and good power quality.

In recent works on DPC, there is a growing use of the extended *p-q* theory to eliminate the second-order power oscillation of PWM rectifiers in unbalanced grids. Different from the classic *p-q* theory, the extended *p-q* theory defines a new variable $\mathbf{T}$ as the product of the quadrature voltage space vector and the conjugate of the current space vector. The new "extended reactive power" is then defined as the real part of the complex power $\mathbf{T}$ as

$$q^{ext} = \frac{3}{2}\mathrm{Re}\left(\mathbf{T}\right) = \frac{3}{2}\mathrm{Re}\left(\mathbf{e}' \cdot \mathbf{i}^{*}\right). \tag{32}$$

The quadrature grid voltage $\mathbf{e}'$ can be expressed as

$$\mathbf{e}' = E^{+}e^{j(\omega t - 90^{\circ})} + E^{-}e^{-j(\omega t - 90^{\circ})} = -jE^{+}e^{j\omega t} + jE^{-}e^{-j\omega t}. \tag{33}$$

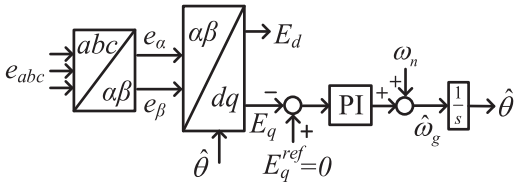

Fig. 23. Structure of an SRF-PLL.

Replacing (33) into (32), the extended reactive power is obtained as

$$q^{\text{ext}} = Q_0^{\text{ext}} + Q_{c2}^{\text{ext}} \cos(2\omega t) + Q_{s2}^{\text{ext}} \sin(2\omega t) \tag{34}$$

where

$$\begin{pmatrix} Q_0^{\text{ext}} \\ Q_{c2}^{\text{ext}} \\ Q_{s2}^{\text{ext}} \end{pmatrix} = \frac{3}{2} \begin{pmatrix} E_d^+ & -E_d^+ & -E_q^- & E_d^- \\ -E_q^- & E_d^- & E_q^+ & -E_d^+ \\ E_d^- & E_q^- & E_d^+ & E_q^+ \end{pmatrix}. \tag{35}$$

Comparing (29) and (35), it is observed that $P_{s2} = -Q_{c2}^{\text{ext}}$ and $P_{c2} = Q_{s2}^{\text{ext}}$, which indicate that the active power ripples have the same magnitude as reactive power ripples. Therefore, the nullification of active power ripples will lead to the elimination of reactive power ripples, which cannot be achieved with the classic instantaneous power theory.

In fact, the two reactive power definitions work the same in balanced grids. An in-depth analysis of their relationship in unbalanced grids is carried out in [110]. It is found that DPCs derived from both definitions are equivalent. By adding extra compensation terms to the power reference, the original reactive power provides the same active power oscillation cancelation as the extended reactive power. However, the acquisition of the compensation terms is complicated due to the use of sequence extraction.

B. Sequence Extraction and Synchronization

To obtain the phase or the frequency of the supply voltage, many PLL techniques have been developed in past decades [111]. The synchronous rotating frame PLL (SRF-PLL) is a standard grid synchronization technique in three-phase applications, as shown in Fig. 23. However, this conventional method is deficient in unbalanced and/or distorted conditions due to the appearance of negative-sequence and harmonic components. To solve this, modified PLL techniques with additional filters have been proposed to reject the interaction between the fundamental-frequency positive-sequence (FFPS) and the fundamental-frequency negative-sequence (FFNS) and/or harmonic components [112], [113].

A double SRF-PLL was proposed to improve the conventional SRF-PLL, as shown in Fig. 24. This synchronization system utilizes two SRFs rotating at the same angular speed but in the opposite direction and a decoupling network to separate FFPS and FFNS components. As a result, the voltage imbalance has no steady-state negative impact on PLL performance. Moreover, the application of several SRF-PLLs in targeted harmonic frequencies creates the multiple-SRF-based PLL that alleviates the

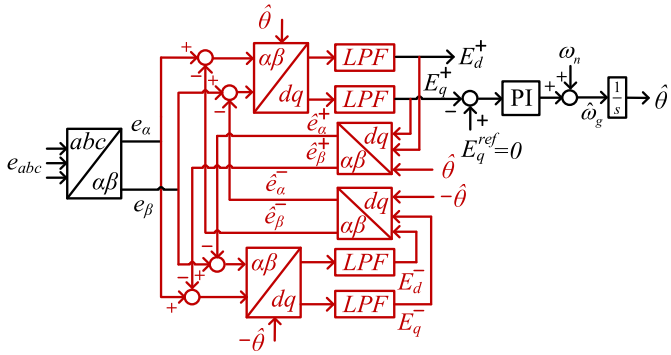

Fig. 24. Structure of a double SRF-PLL.

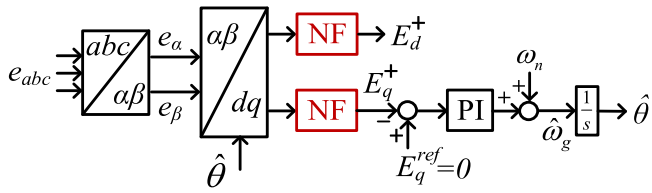

Fig. 25. Structure of an NF-based PLL.

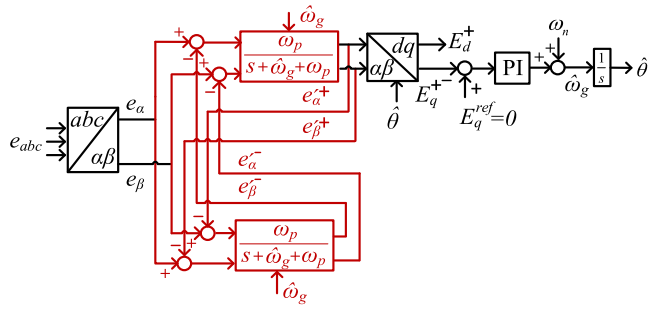

Fig. 26. Structure of a CCF-based PLL.

oscillation of estimated quality caused by harmonic contamination. However, this approach causes a considerable increase in the computational burden [114].

The NF is a popular technique of selective cancelation of unbalanced and/or harmonic components, as it has a high attenuation within a narrow band of frequencies and passes all other components with negligible attenuation. A simple structure is shown in Fig. 25. To achieve sequence detection, the notching frequency of NFs is set at the frequency of unwanted ripples. Usually, three NFs tuned at 2nd-, 6th-, and 12th-fundamental frequency are implemented in either cascaded or parallel structure. The common problem of NFs is the tradeoff between the filtering capability and the computational burden [115].

A complex-coefficient filter (CCF) is another option for the selective extraction of components. The typical structure of the CCF-based PLL is shown in Fig. 26. It offers a unity gain and zero phase shift at the selected frequency and imposing deep attenuation at other frequencies. Due to its asymmetrical frequency response around zero frequencies, CCF makes a distinction between positive- and negative-sequence of the same frequency. Therefore, CCF provides a fast response for real-time signal extraction without symmetrical component methods or complicated rotating frame transformations. Applying several

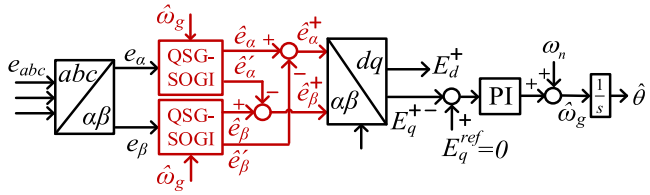

Fig. 27. Structure of the PLL based on double SOGIs.

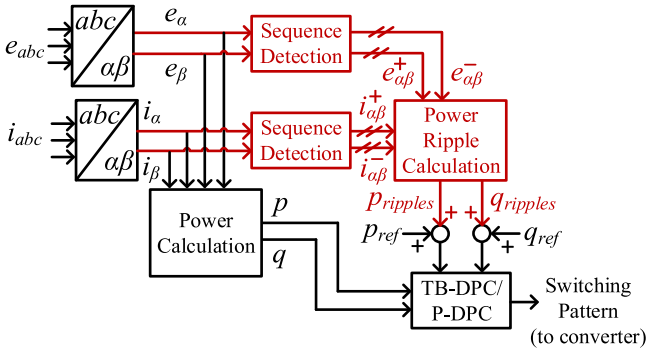

Fig. 28. Structure of a DPC with power ripple compensation.

CCFs for a specified sequence of frequencies creates the multiple CCF. Such a filtering system is capable of extracting FFPS, FFNS, and other harmonic components to address the unbalanced and/or distorted conditions [116].

The double DSOGI is a sequence detection method applied in the two-phase stationary frame. The DSOGI is employed to filter the original two-phase signal and obtain the quadrature counterpart using QSG. The two signals act as inputs to estimate the positive- and negative-sequence components based on the instantaneous symmetrical component method. The resonance frequency of two QSG-SOGIs is set as the grid frequency to obtain the unity gain as well as 0° and 90° phase shift, respectively. Fig. 27 shows the general structure of the sequence detection technique based on the DSOGI [81], [117].

When the fundamental frequency is time-invariant, filters can provide accurate sequence extraction. However, in practice, the fundamental frequency may fluctuate in a certain range. Although the extraction error may be neglected for a slight frequency excursion, significant deterioration will occur under a large frequency fluctuation. To tackle this issue, frequency adaptive approaches are suggested. The common solution is to implement a PLL or a frequency-locked loop on either phase of the two-phase positive-sequence signal to detect the grid frequency and dynamically modify the resonant frequency of filters [80], [118], [119].

C. Power Ripple Compensation

Adding compensation terms to the power reference is a popular technique to attenuate the current distortion and the power fluctuation in unbalanced grids. Fig. 28 shows the general structure. In [15], [16], [61], and [120], based on the power analysis in the α-β stationary frame, the distorted terms are added to the power reference to achieve three individual control targets under

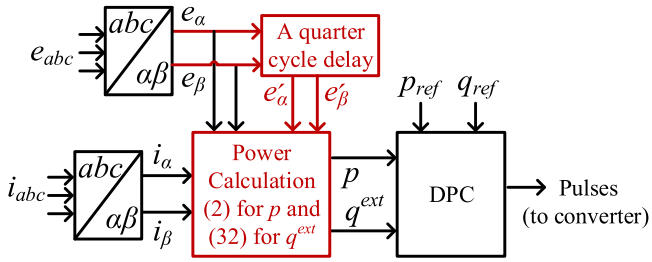

Fig. 29. Structure of a DPC based on the extended p-q theory.

unbalanced grid conditions (i.e., no negative-sequence current, smooth active power, or smooth reactive power). However, these control targets are contradictory to each other, which means that achieving a certain target will jeopardize the performance of other control targets. A similar compensation technique in the d-q frame was implemented to achieve symmetrical grid currents at the expense of increased power oscillation in [121]. In [107], the flexible P-DPC of voltage source inverter under unbalanced grid conditions is proposed. A proportional-integral-resonant controller is used to regulate the double-frequency power ripples. Based on the instantaneous power analysis in the α-β frame, the generalized power reference compensations are calculated as the weighted sum of the given power reference and the power ripple term. Three different control targets are implemented to balance the current negative sequence, the active power ripples, and the reactive power ripples. However, the technique is complex as it requires the positive- and negative-sequence voltages/currents and the third-harmonic current for the power term calculation. To eliminate the sequence separation of voltages/currents and the complex calculation of power compensating terms, a reduced-order vector integrator is introduced to regulate the power pulsations in [122]. The corresponding voltage reference is added to the output of the PI controller regulating the average active and reactive power. SVM is applied to create switching pulses of the PWM converter. Despite its simplicity, the proposed method is sensitive to model parameters due to the use of the feedforward and the proportional terms in calculating the voltage reference.

Approaches using the extended p-q theory for the unbalanced operation of power converters were proposed in [30], [42], [43], [60], and [123]. The general structure is shown in Fig. 29. A comprehensive review of TB-DPC with the original or the extended p-q theories is provided in [124]. Results show that the DPC with the extended p-q theory is able to restrain the current distortion and maintain a good power regulation. The comparative study of DPC methods using the original or the extended p-q theory [110] further indicates that the compensation terms of oscillating powers calculated using the original p-q theory are intrinsically contained in the instantaneous power obtained using the extended p-q theory, which makes the DPC developed in both theories equivalent. Nevertheless, the use of the extended reactive power term makes it straightforward to compensate for the power oscillation without calculating complex ripple terms.

TABLE III
COMPARISON OF CLASSIC DPC STRATEGIES

	Direct Power Control Strategies					
	Voltage-based TB-DPC	Voltage Sensorless TB-DPC	DPC-SVM	SMC-based DPC	3-vector FCS-P-DPC	Deadbeat P-DPC
POWER RIPPLE	High	High	Medium	Medium	Low	Low
CURRENT THD	High	High	Medium	Medium	Low	Low
RESPONSE TIME	Fast	Fast	Fast	Medium	Fast	Medium
SENSITIVITY	Low	Medium	Low	Medium	Low	High
COMPLEXITY	Low	Low	Low	High	High	Medium
SWITCHING FREQUENCY	Variable	Variable	Constant; Programmable	Constant; Programmable	Variable	Constant; Programmable
REFERENCES	[24]	[28]	[7]	[10]	[53]	[59]

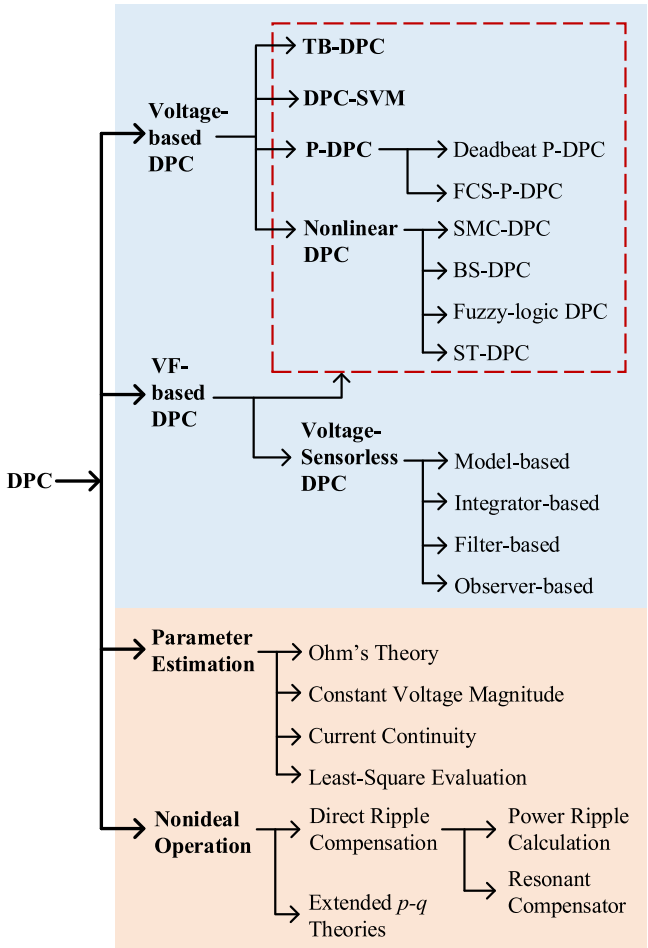

Fig. 30. Family tree of DPC strategies.

IX. COMPARISON OF TYPICAL DPC METHODS

Based on the above discussion, the family tree of various DPC strategies is revealed in Fig. 30. Typical DPC methods are identified as TB-DPC, DPC-SVM, P-DPC, SMC-based DPC, and voltage-sensorless DPC. Strategies under the voltage-based DPC category (highlighted by the dotted red block) are equally appliable using the VF concept. Additionally, voltage-sensorless DPC is another important subcategory of the VF-based strategy. Two critical operating issues are summarized as parameter estimation and nonideal operation. Since a large number of DPC methods have been proposed and verified, the comparative study focuses on the performance of the aforementioned typical methods in this section. Key findings are summarized in Table III.

Classic DPC strategies show some difference in steady-state performance in terms of power ripple and current THD. The power ripple and current THD of TB-DPC approaches are comparably high, as the predefined vectors may not be the optimized ones. Besides, the application of a single vector per control cycle results in large over-regulation of active/reactive power. Due to the removal of the source voltage sensor, the voltage-sensorless TB-DPC is more noise-robust. However, the direct use of inductance for power estimation makes the voltage-sensorless TB-DPC more sensitive to parameter variation. DPC-SVM shows some improvement in steady-state performance. The use of SVM ensures a constant switching frequency. The higher switching frequency can be programmed for better steady-state performance at the expense of higher switching losses. DPC-SVM is robust to parameter variation since the use of linear controllers for reference calculation restrains the impact of parameter inaccuracy. SMC-based DPC shows similar steady-state performance as DPC-SVM. However, it is less robust to parameter variation than DPC-SVM because the SMC rule depends on the system parameters. The switching frequency of SMC-based DPC is also programmable due to the use of SVM for reference synthesis. The multivector FCS-P-DPC shows the best steady-state performance, as the use of objective function ensures the selection of optimal vectors and the acquisition of an optimized duty cycle in each control cycle. However, its switching frequency is relatively higher than that of TB-DPC strategies due to the increased number of commutations in each control cycle. Deadbeat P-DPC calculates the optimal converter voltage vector to ensure the absolute zero power error, which guarantees a good reference tracking performance. Moreover, the deployment of SVM leads to constant switching frequency. However, due to the direct use of system parameters in obtaining

the reference, deadbeat P-DPC is sensitive to parameter variation and sensor inaccuracy.

The dynamic performance of various DPC strategies shows little difference. In general, higher control complexity results in slower dynamics. Therefore, the response time of multiple-vector FCS-P-DPC, deadbeat P-DPC, and SMC-based DPC is slightly slower than the other three simple options. This difference is largely negligible if high-speed control units are employed.

X. Applications of DPC

In addition to three-phase PWM rectifiers, DPC is a favorable control solution in many other power electronics systems. This section discusses other applications of DPC strategies in academia and industry.

A. Doubly Fed Induction Generators (DFIG)

DPC has been widely applied in DFIG, due to its simplicity and fast response. Existing literature covers aspects of modeling [125], stability analysis [126], and control development [127]–[155]. Although the models of DFIG and three-phase PWM rectifiers are different, their DPC implementation is quite similar. Hence, the classification in Fig. 30 can be utilized to facilitate the discussion in this section.

TB-DPC methods are first proposed as an alternative to DTC [127]–[130]. Since the performance of DPC relies on the stator flux position rather than the rotor flux position, it is easier to implement and more robust to machine parameter variations than DTC.

DPC-SVM is investigated to obtain constant switching frequency and eliminate the predefined switching table. Zhou *et al.* [131] introduce a typical implementation similar to the one in [8] and address the unbalanced operation using two proportional-resonant controllers. In [16], an improved DPC-SVM is implemented in the synchronous reference frame to remove the PLL and associated instability issues. Gao *et al.* [132] extend the GVM-DPC proposed in [38] for DFIG applications. The method uses PI regulators to compensate for the power error, hence reducing the reliance on the machine model in obtaining rotor voltage reference. In [133], the standard SMC is implemented with DPC to calculate the equivalent rotor voltage reference synthesized by SVM without any synchronous coordinate transformation.

Many P-DPC strategies have been introduced to improve the control performance of DFIG. Based on the principle discussed in Section V-A, FCS-P-DPC takes advantage of finite switching states of converters. Optimal vector(s) is selected based on the rule of power error minimization. Single-vector approaches are introduced in [134] and [135]. The low-complexity variant is presented in [136]. Several three vectors' approaches are introduced to improve power tracking performance [137]–[141]. The low-complexity variant is presented in [142]. Zarei *et al.* [143] propose a four-vector approach consisting of two zero and two adjacent active vectors to obtain the constant switching frequency and low current distortion at the cost of increased switching losses. Based on the principle in Section V-B, several deadbeat P-DPC strategies are proposed to obtain the closed-form rotor voltage reference synthesized by SVM. The method proposed in [144] is a typical solution that directly calculates the required rotor voltage to eliminate the power errors at the end of the following sampling period. Improved methods are proposed to deal with parameter variations [125], [145].

DPC with other nonlinear control techniques is also investigated. A supertwisting (ST) SMC-based DPC is proposed to obtain good transient and steady-state performance [146]. A BS-DPC is presented in [147] under normal and harmonic grid voltage. Another resonant-based BS-DPC is developed for unbalance operation in [148].

Similar to three-phase PWM rectifiers, the unbalanced operation of DFIG is a critical issue, as the current unbalance causes torque pulsations and overheating of machine windings. The first category of solutions promotes the direct power ripple compensation based on either ripple calculation or resonant compensators. For ripple-calculation-based approaches, sequence detectors are implemented in a two-phase rotating or synchronous framework to isolate positive- and negative-sequence components so that selective compensation targets can be established. Typical methods based on this principle include the so-called DPC+ using a switching table [149], the FCS-P-DPC using single or multiple vectors [135], [136], [143], the SMC-based DPC [150], and VM-DPC-based approaches [151]. The other option employs resonant controllers to obtain the targeted compensation term. In general, original controllers for balanced operation are extended by adding resonant compensators for unbalanced operation. As compared with ripple-calculation-based counterparts, resonant-based solutions are simpler in structure and easier to implement due to the omission of sequence detection. Typical methods include resonant controllers tuned at known pulsating frequencies [131], the single-side resonant controller tuned at the twice fundamental frequency [152], second-order resonant controller tuned at twice positive- and negative-sequence frequencies [148], and an NF-based approach for suppressing dc-link voltage ripples [153]. The second category advocates the extended *p-q* theory for intrinsic ripple compensation without additional power ripple calculation or resonant controllers. In [154], the extended reactive power is adopted to achieve constant stator active power, constant extended reactive power, and sinusoidal stator currents. The extended active power is defined and utilized to establish an SMC-based DPC for sinusoidal stator currents and torque ripple cancelation in [155].

B. Multilevel Converters

Recently, some studies look into the application of DPC in multilevel converters. Since the possible vectors generated by a multilevel converter increases overproportionally to the number of levels, the challenge of DPC implementation is the effective vector evaluation and selection. A general approach applicable to any multilevel converter topology of any number of levels is proposed in [156]. This method simplifies the vector selection by considering the closest subset of two-level voltage vectors to the present switching state and addresses the sensitivity issue by using a derivative estimator and a VF observer. Applications to

specific multilevel converters with the given number of levels are also proposed, such as three-level neutral point clamped converter (NPC) [157]–[159], three-level T-type inverter [160], and five-level active NPC [161].

C. Active Power Filters (APFs)

Specific applications of DPC for shunt APFs are presented. Chen and JoÓs [23] improve the classic VF-based TB-DPC by using two low-pass filters and subtraction logics to obtain power ripples. Based on the classic DPC-SVM, additional high-pass filters are used to obtain reference terms for power ripple compensation [37]. A recent work presents an ST-SMC-based DPC with SVM [162]. Another deadbeat P-DPC is implemented to operate an APF integrated with a quasi-Z-source inverter for active power decoupling in [163].

D. Single-Phase Converters

Although DPC has been extensively investigated in a three-phase system, only a few applications have been investigated for single-phase converters. A deadbeat P-DPC with online inductance estimation is proposed for a single-phase PWM rectifier in [164]. An FCS-P-DPC is developed for a traction line-side converter in a high-speed railway system in [165].

XI. Conclusion

This article conducts a comprehensive survey on the state-of-the-art DPC strategies applied for three-phase two-level PWM converters. This category of control strategies is gaining increasing attention in both industry and academia. Among different variants, the P-DPC is the most promising option benefiting from the latest advances in MPC techniques. Sophisticated solutions considering the observation of the source voltage/flux for the voltage-sensorless control and the estimation of circuit parameters for the robust control will continue to expand the frontier of DPCs for better performance. In addition, adapting the DPC in nonideal source conditions remains to be a concerning matter in exerting the full potential of DPCs. It is important to highlight that DPC can be applied for not only three-phase two-level PWM converters but also other power-electronics-driven systems such as DFIG, multilevel converters, APFs, and single-phase converters.

References

[1] B. Singh, B. N. Singh, A. Chandra, K. Al-Haddad, A. Pandey, and D. P. Kothari, "A review of three-phase improved power quality AC-DC converters," *IEEE Trans. Ind. Electron.,* vol. 51, no. 3, pp. 641–660, Jun. 2004.

[2] J. R. Rodriguez, J. W. Dixon, J. R. Espinoza, J. Pontt, and P. Lezana, "PWM regenerative rectifiers: State of the art," *IEEE Trans. Ind. Electron.,* vol. 52, no. 1, pp. 5–22, Feb. 2005.

[3] F. Blaabjerg, R. Teodorescu, M. Liserre, and A. V. Timbus, "Overview of control and grid synchronization for distributed power generation systems," *IEEE Trans. Ind. Electron.,* vol. 53, no. 5, pp. 1398–1409, Oct. 2006.

[4] M. Malinowski, M. P. Kazmierkowski, and A. M. Trzynadlowski, "A comparative study of control techniques for PWM rectifiers in AC adjustable speed drives," *IEEE Trans. Power Electron.,* vol. 18, no. 6, pp. 1390–1396, Nov. 2003.

[5] Z. Xie, W. Wu, Y. Chen, and W. Gong, "Admittance-Based stability comparative analysis of grid-connected inverters with direct power control and closed-loop current control," *IEEE Trans. Ind. Electron.,* to be published.

[6] T. Ohnishi, "Three phase PWM converter/inverter by means of instantaneous active and reactive power control," in *Proc. Int. Conf. Ind. Electron., Control Instrum.*, Oct. 28–Nov. 1, 1991, vol. 1, pp. 819–824.

[7] M. Malinowski, M. Jasinski, and M. P. Kazmierkowski, "Simple direct power control of three-phase PWM rectifier using space-vector modulation (DPC-SVM)," *IEEE Trans. Ind. Electron.,* vol. 51, no. 2, pp. 447–454, Apr. 2004.

[8] M. P. Kazmierkowski, M. Jasinski, and G. Wrona, "DSP-Based control of grid-connected power converters operating under grid distortions," *IEEE Trans. Ind. Inf.,* vol. 7, no. 2, pp. 204–211, May 2011.

[9] P. CortÉs, J. RodrÍguez, P. Antoniewicz, and M. Kazmierkowski, "Direct power control of an AFE using predictive control," *IEEE Trans. Power Electron.,* vol. 23, no. 5, pp. 2516–2523, Sep. 2008.

[10] J. Hu, L. Shang, Y. He, and Z. Q. Zhu, "Direct active and reactive power regulation of grid-connected DC/AC converters using sliding mode control approach," *IEEE Trans. Power Electron.,* vol. 26, no. 1, pp. 210–222, Jan. 2011.

[11] R. Wai and Y. Yang, "Design of backstepping direct power control for three-phase PWM rectifier," *IEEE Trans. Ind. Appl.,* vol. 55, no. 3, pp. 3160–3173, May/Jun. 2019.

[12] J. Ge, Z. Zhao, L. Yuan, T. Lu, and F. He, "Direct power control based on natural switching surface for three-phase PWM rectifiers," *IEEE Trans. Power Electron.,* vol. 30, no. 6, pp. 2918–2922, Jun. 2015.

[13] A. Bouafia, F. Krim, and J. Gaubert, "Fuzzy-Logic-Based switching state selection for direct power control of three-phase PWM rectifier," *IEEE Trans. Ind. Electron.,* vol. 56, no. 6, pp. 1984–1992, Jun. 2009.

[14] H. Yang, Y. Zhang, J. Liang, J. Liu, N. Zhang, and P. D. Walker, "Robust deadbeat predictive power control with a discrete-time disturbance observer for PWM rectifiers under unbalanced grid conditions," *IEEE Trans. Power Electron.,* vol. 34, no. 1, pp. 287–300, Jan. 2019.

[15] L. Shang, D. Sun, and J. Hu, "Sliding-mode-based direct power control of grid-connected voltage-sourced inverters under unbalanced network conditions," *IET Power Electron,* vol. 4, no. 5, pp. 570–579, May 2011.

[16] D. Sun, X. Wang, and Y. Fang, "Backstepping direct power control without phase-locked loop of AC/DC converter under both balanced and unbalanced grid conditions," *IET Power Electron,* vol. 9, no. 8, pp. 1614–1624, Jun. 2016.

[17] X. H. Wu, S. K. Panda, and J. X. Xu, "Analysis of the instantaneous power flow for three-phase PWM boost rectifier under unbalanced supply voltage conditions," *IEEE Trans. Power Electron.,* vol. 23, no. 4, pp. 1679–1691, Jul. 2008.

[18] H. Akagi, Y. Kanazawa, and A. Nabae, "Instantaneous reactive power compensators comprising switching devices without energy storage components," *IEEE Trans. Ind. Appl.,* vol. IA-20, no. 3, pp. 625–630, May 1984.

[19] F. Z. Peng and J.-S. Lai, " Generalized instantaneous reactive power theory for three-phase power systems," *IEEE Trans. Instrum. Meas.,* vol. 45, no. 1, pp. 293–297, Feb. 1996.

[20] A. Baktash, A. Vahedi, and M. A. S. Masoum, "Improved switching table for direct power control of three-phase PWM rectifier," in *Proc. Australas. Univ. Power Eng. Conf.*, Dec. 9–12, 2007, pp. 1–5.

[21] A. Bouafia, J. Gaubert, and F. Krim, "Analysis and design of new switching table for direct power control of three-phase PWM rectifier," in *Proc. 13th Int. Power Electron. Motion Control Conf.*, Sep. 1–3, 2008, pp. 703–709.

[22] J. Eloy-Garcia and R. Alves, "DSP-based direct power control of a VSC with voltage angle estimation," in *Proc. IEEE/PES Transmiss. Distrib. Conf. Expo., Latin Am.*, Aug. 15–18, 2006, pp. 1–5.

[23] B. S. Chen and G. JoÓs, "Direct power control of active filters with averaged switching frequency regulation," *IEEE Trans. Power Electron.,* vol. 23, no. 6, pp. 2729–2737, Nov. 2008.

[24] Y. Zhang, Z. Li, Y. Zhang, W. Xie, Z. Piao, and C. Hu, "Performance improvement of direct power control of PWM rectifier with simple calculation," *IEEE Trans. Power Electron.,* vol. 28, no. 7, pp. 3428–3437, Jul. 2013.

[25] T. Noguchi, H. Tomiki, S. Kondo, and I. Takahashi, "Direct power control of PWM converter without power-source voltage sensors," *IEEE Trans. Ind. Appl.,* vol. 34, no. 3, pp. 473–479, May/Jun. 1998.

[26] M. Malinowski, M. P. Kazmierkowski, S. Hansen, F. Blaabjerg, and G. D. Marques, "Virtual-flux-based direct power control of three-phase PWM rectifiers," *IEEE Trans. Ind. Appl.,* vol. 37, no. 4, pp. 1019–1027, Jul./Aug. 2001.

[27] J. Hu, "Improved dead-beat predictive DPC strategy of grid-connected DC–AC converters with switching loss minimization and delay compensations," *IEEE Trans. Ind. Inf.,* vol. 9, no. 2, pp. 728–738, May 2013.

[28] A. M. Razali, M. A. Rahman, G. George, and N. A. Rahim, "Analysis and design of new switching lookup table for virtual flux direct power control of grid-connected three-phase PWM AC–DC converter," *IEEE Trans. Ind. Appl.,* vol. 51, no. 2, pp. 1189–1200, Mar./Apr. 2015.

[29] J. G. Norniella *et al.*, "Improving the dynamics of virtual-flux-based control of three-phase active rectifiers," *IEEE Trans. Ind. Electron.,* vol. 61, no. 1, pp. 177–187, Jan. 2014.

[30] Y. Zhang and C. Qu, "Table-based direct power control for three-phase AC/DC converters under unbalanced grid voltages," *IEEE Trans. Power Electron.,* vol. 30, no. 12, pp. 7090–7099, Dec. 2015.

[31] J. Alonso-Martínez, J. E. Carrasco, and S. Arnaltes, "Table-based direct power control: A critical review for microgrid applications," *IEEE Trans. Power Electron.,* vol. 25, no. 12, pp. 2949–2961, Dec. 2010.

[32] D. Zhi, L. Xu, and B. W. Williams, "Improved direct power control of grid-connected DC/AC converters," *IEEE Trans. Power Electron.,* vol. 24, no. 5, pp. 1280–1292, May 2009.

[33] G. Escobar, A. M. Stankovic, J. M. Carrasco, E. Galvan, and R. Ortega, "Analysis and design of direct power control (DPC) for a three phase synchronous rectifier via output regulation subspaces," *IEEE Trans. Power Electron.,* vol. 18, no. 3, pp. 823–830, May 2003.

[34] Y. Zhang, W. Xie, and Y. Zhang, "Deadbeat direct power control of three-phase pulse-width modulation rectifiers," *IET Power Electron,* vol. 7, no. 6, pp. 1340–1346, Jun. 2014.

[35] S. Vazquez, J. A. Sanchez, J. M. Carrasco, J. I. Leon, and E. Galvan, "A model-based direct power control for three-phase power converters," *IEEE Trans. Ind. Electron.,* vol. 55, no. 4, pp. 1647–1657, Apr. 2008.

[36] H. A. Hamed, A. F. Abdou, S. Acharya, M. S. E. Moursi, and E. E. El-Kholy, "A novel dynamic switching table based direct power control strategy for grid connected converters," *IEEE Trans. Energy Convers.,* vol. 33, no. 3, pp. 1086–1097, Sep. 2018.

[37] M. Cichowlas, M. Malinowski, M. P. Kazmierkowski, D. L. Sobczuk, P. Rodriguez, and J. Pou, "Active filtering function of three-phase PWM boost rectifier under different line voltage conditions," *IEEE Trans. Ind. Electron.,* vol. 52, no. 2, pp. 410–419, Apr. 2005.

[38] Y. Gui, C. Kim, C. C. Chung, J. M. Guerrero, Y. Guan, and J. C. Vasquez, "Improved direct power control for grid-connected voltage source converters," *IEEE Trans. Ind. Electron.,* vol. 65, no. 10, pp. 8041–8051, Oct. 2018.

[39] S. Kwak and J. Park, "Model-Predictive direct power control with vector preselection technique for highly efficient active rectifiers," *IEEE Trans. Ind. Inf.,* vol. 11, no. 1, pp. 44–52, Feb. 2015.

[40] J. Hu, J. Zhu, and D. G. Dorrell, "Model predictive control of grid-connected inverters for PV systems with flexible power regulation and switching frequency reduction," *IEEE Trans. Ind. Appl.,* vol. 51, no. 1, pp. 587–594, Jan./Feb. 2015.

[41] Y. Zhang, W. Xie, Z. Li, and Y. Zhang, "Model predictive direct power control of a PWM rectifier with duty cycle optimization," *IEEE Trans. Power Electron.,* vol. 28, no. 11, pp. 5343–5351, Nov. 2013.

[42] Y. Zhang and C. Qu, "Model predictive direct power control of PWM rectifiers under unbalanced network conditions," *IEEE Trans. Ind. Electron.,* vol. 62, no. 7, pp. 4011–4022, Jul. 2015.

[43] Y. Zhang, C. Qu, and J. Gao, "Performance improvement of direct power control of PWM rectifier under unbalanced network," *IEEE Trans. Power Electron.,* vol. 32, no. 3, pp. 2319–2328, Mar. 2017.

[44] A. M. Bozorgi, H. Gholami-Khesht, M. Farasat, S. Mehraeen, and M. Monfared, "Model predictive direct power control of three-phase grid-connected converters with fuzzy-based duty cycle modulation," *IEEE Trans. Ind. Appl.,* vol. 54, no. 5, pp. 4875–4885, Sep./Oct. 2018.

[45] Y. Zhang, Y. Peng, and H. Yang, "Performance improvement of two-vectors-based model predictive control of PWM rectifier," *IEEE Trans. Power Electron.,* vol. 31, no. 8, pp. 6016–6030, Aug. 2016.

[46] S. Aurtenechea Larrinaga, M. A. R. Vidal, E. Oyarbide, and J. R. T. Apraiz, "Predictive control strategy for DC/AC converters based on direct power control," *IEEE Trans. Ind. Electron.,* vol. 54, no. 3, pp. 1261–1271, Jun. 2007.

[47] P. Antoniewicz and M. P. Kazmierkowski, "Virtual-flux-based predictive direct power control of AC/DC converters with online inductance estimation," *IEEE Trans. Ind. Electron.,* vol. 55, no. 12, pp. 4381–4390, Dec. 2008.

[48] J. Hu and Z. Q. Zhu, "Investigation on switching patterns of direct power control strategies for grid-connected DC–AC converters based on power variation rates," *IEEE Trans. Power Electron.,* vol. 26, no. 12, pp. 3582–3598, Dec. 2011.

[49] J. Hu and Z. Q. Zhu, "Improved voltage-vector sequences on dead-beat predictive direct power control of reversible three-phase grid-connected voltage-source converters," *IEEE Trans. Power Electron.,* vol. 28, no. 1, pp. 254–267, Jan. 2013.

[50] S. Vazquez, A. Marquez, R. Aguilera, D. Quevedo, J. I. Leon, and L. G. Franquelo, "Predictive optimal switching sequence direct power control for grid-connected power converters," *IEEE Trans. Ind. Electron.,* vol. 62, no. 4, pp. 2010–2020, Apr. 2015.

[51] Z. Song, W. Chen, and C. Xia, "Predictive direct power control for three-phase grid-connected converters without sector information and voltage vector selection," *IEEE Trans. Power Electron.,* vol. 29, no. 10, pp. 5518–5531, Oct. 2014.

[52] Z. Zhang, H. Fang, F. Gao, J. Rodríguez, and R. Kennel, "Multiple-vector model predictive power control for grid-tied wind turbine system with enhanced steady-state control performance," *IEEE Trans. Ind. Electron.,* vol. 64, no. 8, pp. 6287–6298, Aug. 2017.

[53] D. Zhou, P. Tu, and Y. Tang, "Multivector model predictive power control of three-phase rectifiers with reduced power ripples under nonideal grid conditions," *IEEE Trans. Ind. Electron.,* vol. 65, no. 9, pp. 6850–6859, Sep. 2018.

[54] S. Yan, J. Chen, T. Yang, and S. Y. Hui, "Improving the performance of direct power control using duty cycle optimization," *IEEE Trans. Power Electron.,* vol. 34, no. 9, pp. 9213–9223, Sep. 2019.

[55] S. Yan, J. Chen, S. Tan, and S. Y. Hui, "A new geometric vector optimization of predictive direct power control," *IEEE Trans. Power Electron.,* vol. 35, no. 5, pp. 5427–5436, May 2020.

[56] Y. Zhang and W. Xie, "Low complexity model predictive control—Single vector-based approach," *IEEE Trans. Power Electron.,* vol. 29, no. 10, pp. 5532–5541, Oct. 2014.

[57] Y. Zhang, W. Xie, Z. Li, and Y. Zhang, "Low-complexity model predictive power control: Double-vector-based approach," *IEEE Trans. Ind. Electron.,* vol. 61, no. 11, pp. 5871–5880, Nov. 2014.

[58] J. A. Restrepo, J. M. Aller, J. C. Viola, A. Bueno, and T. G. Habetler, "Optimum space vector computation technique for direct power control," *IEEE Trans. Power Electron.,* vol. 24, no. 6, pp. 1637–1645, Jun. 2009.

[59] A. Bouafia, J. Gaubert, and F. Krim, "Predictive direct power control of three-phase pulsewidth modulation (PWM) rectifier using space-vector modulation (SVM)," *IEEE Trans. Power Electron.,* vol. 25, no. 1, pp. 228–236, Jan. 2010.

[60] Y. Zhang and C. Qu, "Direct power control of a pulse width modulation rectifier using space vector modulation under unbalanced grid voltages," *IEEE Trans. Power Electron.,* vol. 30, no. 10, pp. 5892–5901, Oct. 2015.

[61] Y. Zhang, J. Liu, H. Yang, and J. Gao, "Direct power control of pulsewidth modulated rectifiers without DC voltage oscillations under unbalanced grid conditions," *IEEE Trans. Ind. Electron.,* vol. 65, no. 10, pp. 7900–7910, Oct. 2018.

[62] Y. Cho and K. Lee, "Virtual-Flux-Based predictive direct power control of three-phase PWM rectifiers with fast dynamic response," *IEEE Trans. Power Electron.,* vol. 31, no. 4, pp. 3348–3359, Apr. 2016.

[63] Y. Zhang, Y. Peng, and C. Qu, "Model predictive control and direct power control for PWM rectifiers with active power ripple minimization," *IEEE Trans. Ind. Appl.,* vol. 52, no. 6, pp. 4909–4918, Nov./Dec. 2016.

[64] D. Choi and K. Lee, "Dynamic performance improvement of AC/DC converter using model predictive direct power control with finite control set," *IEEE Trans. Ind. Electron.,* vol. 62, no. 2, pp. 757–767, Feb. 2015.

[65] H. Li, M. Lin, and G. Yang, "Fuzzy logic based model predictive direct power control of three phase PWM rectifier," in *Proc. 21st Int. Conf. Elect. Mach. Syst.*, Oct. 7–10, 2018, pp. 2431–2435.

[66] D. E. Quevedo, R. P. Aguilera, M. A. Perez, P. Cortes, and R. Lizana, "Model predictive control of an AFE rectifier with dynamic references," *IEEE Trans. Power Electron.,* vol. 27, no. 7, pp. 3128–3136, Jul. 2012.

[67] B. Arif, L. Tarisciotti, P. Zanchetta, J. C. Clare, and M. Degano, "Grid parameter estimation using model predictive direct power control," *IEEE Trans. Ind. Appl.,* vol. 51, no. 6, pp. 4614–4622, Nov./Dec. 2015.

[68] J. Holtz, "Sensorless control of induction motor drives," *Proc. IEEE,* vol. 90, no. 8, pp. 1359–1394, Aug. 2002.

[69] Y. Zhao, C. Wei, Z. Zhang, and W. Qiao, "A review on position/speed sensorless control for permanent-magnet synchronous machine-based wind energy conversion systems," *IEEE J. Emerg. Sel. Topics Power Electron.,* vol. 1, no. 4, pp. 203–216, Dec. 2013.

[70] H. Jun and W. Bin, "New integration algorithms for estimating motor flux over a wide speed range," *IEEE Trans. Power Electron.,* vol. 13, no. 5, pp. 969–977, Sep. 1998.

[71] M.-H. Shin, D.-S. Hyun, S.-B. Cho, and S.-Y. Choe, "An improved stator flux estimation for speed sensorless stator flux orientation control of induction motors," *IEEE Trans. Power Electron.,* vol. 15, no. 2, pp. 312–318, Mar. 2000.

[72] M. Hinkkanen and J. Luomi, "Modified integrator for voltage model flux estimation of induction motors," *IEEE Trans. Ind. Electron.,* vol. 50, no. 4, pp. 818–820, Aug. 2003.

[73] M. Comanescu and L. Xu, "An improved flux observer based on PLL frequency estimator for sensorless vector control of induction motors," *IEEE Trans. Ind. Electron.,* vol. 53, no. 1, pp. 50–56, Feb. 2006.

[74] N. R. N. Idris and A. H. M. Yatim, "An improved stator flux estimation in steady-state operation for direct torque control of induction machines," *IEEE Trans. Ind. Appl.,* vol. 38, no. 1, pp. 110–116, Jan./Feb. 2002.

[75] Z. Zhang *et al.*, "Predictive control with novel virtual-flux estimation for back-to-back power converters," *IEEE Trans. Ind. Electron.,* vol. 62, no. 5, pp. 2823–2834, May 2015.

[76] J. L. Duarte, A. V. Zwam, C. Wijnands, and A. Vandenput, "Reference frames fit for controlling PWM rectifiers," *IEEE Trans. Ind. Electron.,* vol. 46, no. 3, pp. 628–630, Jun. 1999.

[77] S. Bhattacharya, A. Veltman, D. M. Divan, and R. D. Lorenz, "Flux-based active filter controller," *IEEE Trans. Ind. Appl.,* vol. 32, no. 3, pp. 491–502, May/Jun. 1996.

[78] M. Cirrincione, M. Pucci, G. Cirrincione, and G. Capolino, "A new adaptive integration methodology for estimating flux in induction machine drives," *IEEE Trans. Power Electron.,* vol. 19, no. 1, pp. 25–34, Jan. 2004.

[79] M. Zerbo, P. Sicard, and A. Ba-Razzouk, "Accurate adaptive integration algorithms for induction machine drive over a wide speed range," in *Proc. IEEE Int. Conf. Electr. Mach. Drives*, May 2005, pp. 1082–1088.

[80] J. A. Suul, A. Luna, P. Rodriguez, and T. Undeland, "Voltage-sensor-less synchronization to unbalanced grids by frequency-adaptive virtual flux estimation," *IEEE Trans. Ind. Electron.,* vol. 59, no. 7, pp. 2910–2923, Jul. 2012.

[81] J. A. Suul, A. Luna, P. Rodríguez, and T. Undeland, "Virtual-flux-based voltage-sensor-less power control for unbalanced grid conditions," *IEEE Trans. Power Electron.,* vol. 27, no. 9, pp. 4071–4087, Sep. 2012.

[82] Y. Zhang, Z. Wang, J. Jiao, and J. Liu, "Grid-voltage sensorless model predictive control of three-phase PWM rectifier under unbalanced and distorted grid voltages," *IEEE Trans. Power Electron.,* vol. 35, no. 8, pp. 8663–8672, Aug. 2020.

[83] H. Yang, Y. Zhang, and J. Liu, "Frequency-adaptive virtual flux estimator-based predictive power control with suppression of dc voltage ripples under unbalanced network," *IEEE Trans. Ind. Electron.,* vol. 67, no. 10, pp. 8969–8979, Oct. 2020.

[84] M. Hinkkanen, S. E. Saarakkala, H. A. A. Awan, E. Mölsä, and T. Tuovinen, "Observers for sensorless synchronous motor drives: Framework for design and analysis," *IEEE Trans. Ind. Appl.,* vol. 54, no. 6, pp. 6090–6100, Nov./Dec. 2018.

[85] R. Agha Zadeh, A. Ghosh, and G. Ledwich, "Combination of Kalman filter and least-error square techniques in power system," *IEEE Trans. Power Del.,* vol. 25, no. 4, pp. 2868–2880, Oct. 2010.

[86] V. M. Moreno, M. Liserre, A. Pigazo, and A. Dell'Aquila, "A comparative analysis of real-time algorithms for power signal decomposition in multiple synchronous reference frames," *IEEE Trans. Power Electron.,* vol. 22, no. 4, pp. 1280–1289, Jul. 2007.

[87] M. Liserre, A. Pigazo, A. Dell'Aquila, and V. M. Moreno, "An anti-islanding method for single-phase inverters based on a grid voltage sensorless control," *IEEE Trans. Ind. Electron.,* vol. 53, no. 5, pp. 1418–1426, Oct. 2006.

[88] N. Salvatore, A. Caponio, F. Neri, S. Stasi, and G. L. Cascella, "Optimization of delayed-state Kalman-filter-based algorithm via differential evolution for sensorless control of induction motors," *IEEE Trans. Ind. Electron.,* vol. 57, no. 1, pp. 385–394, Jan. 2010.

[89] M. Malinowski and S. Bernet, "A simple voltage sensorless active damping scheme for three-phase PWM converters with an LCL filter," *IEEE Trans. Ind. Electron.,* vol. 55, no. 4, pp. 1876–1880, Apr. 2008.

[90] F. Huerta, D. Pizarro, S. Cobreces, F. J. Rodriguez, C. Giron, and A. Rodriguez, "LQG servo controller for the current control of LCL grid-connected voltage-source converters," *IEEE Trans. Ind. Electron.,* vol. 59, no. 11, pp. 4272–4284, Nov. 2012.

[91] S. Mariethoz and M. Morari, "Explicit model-predictive control of a PWM inverter with an LCL filter," *IEEE Trans. Ind. Electron.,* vol. 56, no. 2, pp. 389–399, Feb. 2009.

[92] K. Lee, T. M. Jahns, T. A. Lipo, and V. Blasko, "New control method including state observer of voltage unbalance for grid voltage-source converters," *IEEE Trans. Ind. Electron.,* vol. 57, no. 6, pp. 2054–2065, Jun. 2010.

[93] R. Kumar, S. Das, P. Syam, and A. K. Chattopadhyay, "Review on model reference adaptive system for sensorless vector control of induction motor drives," *IET Electr. Power Appl.,* vol. 9, no. 7, pp. 496–511, Aug. 2015.

[94] A. Pal, S. Das, and A. K. Chattopadhyay, "An improved rotor flux space vector based MRAS for field-oriented control of induction motor drives," *IEEE Trans. Power Electron.,* vol. 33, no. 6, pp. 5131–5141, Jun. 2018.

[95] W. Xu, A. K. Ebraheem, Y. Liu, J. Zhu, M. G. Hussien, and O. M. Elbabo Mohammed, "An MRAS speed observer based on control winding flux for sensorless control of stand-alone BDFIGs," *IEEE Trans. Power Electron.,* vol. 35, no. 7, pp. 7271–7281, Jul. 2020.

[96] R. G. Tonin, T. Bernardes, J. R. Massing, and H. Pinheiro, "Sliding mode observer for voltage sensorless current control of grid-connected converters," in *Proc. Braz. Power Electron. Conf.*, Oct. 27–31, 2013, pp. 387–392.

[97] L. Guo, N. Jin, Y. Li, and K. Luo, "A model predictive control method for grid-connected power converters without AC voltage sensors," *IEEE Trans. Ind. Electron.,* vol. 68, no. 2, pp. 1299–1310, Feb. 2021.

[98] A. M. Bozorgi, H. Gholami-Khesht, M. Farasat, S. Mehraeen, and M. Monfared, "Voltage sensorless improved model predictive direct power control for three-phase grid-connected converters," in *Proc. IEEE Energy Convers. Congr. Expo.*, Oct. 1–5, 2017, pp. 4957–4963.

[99] H. Gholami-Khesht and M. Monfared, "Deadbeat direct power control for grid connected inverters using a full-order observer," in *Proc. 4th Int. Conf. Electr. Power Energy Convers. Syst.*, Nov. 24–26, 2015, pp. 1–5.

[100] J. R. Fischer, S. A. González, I. Carugati, M. A. Herrán, M. G. Judewicz, and D. O. Carrica, "Robust predictive control of grid-tied converters based on direct power control," *IEEE Trans. Power Electron.,* vol. 29, no. 10, pp. 5634–5643, Oct. 2014.

[101] H. Yang, Y. Zhang, J. Liang, J. Gao, P. D. Walker, and N. Zhang, "Sliding-mode observer based voltage-sensorless model predictive power control of PWM rectifier under unbalanced grid conditions," *IEEE Trans. Ind. Electron.,* vol. 65, no. 7, pp. 5550–5560, Jul. 2018.

[102] X. Xiao, Y. Zhang, X. Song, T. Yildirim, and F. Zhang, "Virtual flux direct power control for PWM rectifiers based on an adaptive sliding mode observer," *IEEE Trans. Ind. Appl.,* vol. 54, no. 5, pp. 5196–5205, Sep./Oct. 2018.

[103] Z. Song, Y. Tian, Z. Yan, and Z. Chen, "Direct power control for three-phase two-level voltage-source rectifiers based on extended-state observation," *IEEE Trans. Ind. Electron.,* vol. 63, no. 7, pp. 4593–4603, Jul. 2016.

[104] J. G. Norniella *et al.*, "Analytic and iterative algorithms for online estimation of coupling inductance in direct power control of three-phase active rectifiers," *IEEE Trans. Power Electron.,* vol. 26, no. 11, pp. 3298–3307, Nov. 2011.

[105] S. Kwak, U. Moon, and J. Park, "Predictive-control-based direct power control with an adaptive parameter identification technique for improved AFE performance," *IEEE Trans. Power Electron.,* vol. 29, no. 11, pp. 6178–6187, Nov. 2014.

[106] Y. Zhang, J. Jiao, and J. Liu, "Direct power control of PWM rectifiers with online inductance identification under unbalanced and distorted network conditions," *IEEE Trans. Power Electron.,* vol. 34, no. 12, pp. 12524–12537, Dec. 2019.

[107] H. Nian, Y. Shen, H. Yang, and Y. Quan, "Flexible grid connection technique of voltage-source inverter under unbalanced grid conditions based on direct power control," *IEEE Trans. Ind. Appl.,* vol. 51, no. 5, pp. 4041–4050, Sep./Oct. 2015.

[108] Y. Komatsu and T. Kawabata, "Characteristics of three phase active power filter using extension pq theory," in *Proc. IEEE Int. Symp. Ind. Electron* ., Jul. 7–11, 1997, vol. 2, pp. 302–307.

[109] Y. Suh and T. A. Lipo, "Modeling and analysis of instantaneous active and reactive power for PWM AC/DC converter under generalized unbalanced network," *IEEE Trans. Power Del.,* vol. 21, no. 3, pp. 1530–1540, Jul. 2006.

[110] Y. Zhang, J. Gao, and C. Qu, "Relationship between two direct power control methods for PWM rectifiers under unbalanced network," *IEEE Trans. Power Electron.,* vol. 32, no. 5, pp. 4084–4094, May 2017.

[111] S. Golestan, J. M. Guerrero, and J. C. Vasquez, "Three-phase PLLs: A review of recent advances," *IEEE Trans. Power Electron.,* vol. 32, no. 3, pp. 1894–1907, Mar. 2017.

[112] S. Golestan, M. Monfared, and F. D. Freijedo, "Design-oriented study of advanced synchronous reference frame phase-locked loops," *IEEE Trans. Power Electron.,* vol. 28, no. 2, pp. 765–778, Feb. 2013.

[113] A. Luna *et al.*, "Grid voltage synchronization for distributed generation systems under grid fault conditions," *IEEE Trans. Ind. Appl.,* vol. 51, no. 4, pp. 3414–3425, Jul./Aug. 2015.

[114] P. Xiao, K. A. Corzine, and G. K. Venayagamoorthy, "Multiple reference frame-based control of three-phase PWM boost rectifiers under unbalanced and distorted input conditions," *IEEE Trans. Power Electron.,* vol. 23, no. 4, pp. 2006–2017, Jul. 2008.

[115] F. Gonzalez-Espin, E. Figueres, and G. Garcera, "An adaptive synchronous-reference-frame phase-locked loop for power quality improvement in a polluted utility grid," *IEEE Trans. Ind. Electron.,* vol. 59, no. 6, pp. 2718–2731, Jun. 2012.

[116] X. Guo, W. Wu, and Z. Chen, "Multiple-complex coefficient-filter-based phase-locked loop and synchronization technique for three-phase grid-interfaced converters in distributed utility networks," *IEEE Trans. Ind. Electron.,* vol. 58, no. 4, pp. 1194–1204, Apr. 2011.

[117] X. Yuan., W. Merk, H. Stemmler, and J. Allmeling, "Stationary-frame generalized integrators for current control of active power filters with zero steady-state error for current harmonics of concern under unbalanced and distorted operating conditions," *IEEE Trans. Ind. Appl.,* vol. 38, no. 2, pp. 523–532, Mar./Apr. 2002.

[118] P. Rodríguez, A. Luna, R. S. Muñoz-Aguilar, I. Etxeberria-Otadui, R. Teodorescu, and F. Blaabjerg, "A stationary reference frame grid synchronization system for three-phase grid-connected power converters under adverse grid conditions," *IEEE Trans. Power Electron.,* vol. 27, no. 1, pp. 99–112, Jan. 2012.

[119] P. Rodríguez, R. Teodorescu, I. Candela, A. V. Timbus, M. Liserre, and F. Blaabjerg, "New positive-sequence voltage detector for grid synchronization of power converters under faulty grid conditions," in *Proc. 37th IEEE Power Electron. Spec. Conf.*, Jun. 18–22, 2006, pp. 1–7.

[120] N. Jin, S. Hu, C. Gan, and Z. Ling, "Finite states model predictive control for fault-tolerant operation of a three-phase bidirectional AC/DC converter under unbalanced grid voltages," *IEEE Trans. Ind. Electron.,* vol. 65, no. 1, pp. 819–829, Jan. 2018.

[121] J. Eloy-Garcia, S. Arnaltes, and J. L. Rodriguez-Amenedo, "Direct power control of voltage source inverters with unbalanced grid voltages," *IET Power Electron.,* vol. 1, no. 3, pp. 395–407, Sep. 2008.

[122] P. Cheng and H. Nian, "Direct power control of voltage source inverter in a virtual synchronous reference frame during frequency variation and network unbalance," *IET Power Electron.,* vol. 9, no. 3, pp. 502–511, 2016.

[123] Y. Zhang, J. Jiao, J. Liu, and J. Gao, "Direct power control of PWM rectifier with feedforward compensation of DC-bus voltage ripple under unbalanced grid conditions," *IEEE Trans. Ind. Appl.,* vol. 55, no. 3, pp. 2890–2901, May/Jun. 2019.

[124] S. S. Lee and Y. E. Heng, "Table-based DPC for grid connected VSC under unbalanced and distorted grid voltages: Review and optimal method," *Renewable Sustain. Energy Rev.,* vol. 76, pp. 51–61, 2017.

[125] R. Errouissi, A. Al-Durra, S. M. Muyeen, S. Leng, and F. Blaabjerg, "Offset-free direct power control of DFIG under continuous-time model predictive control," *IEEE Trans. Power Electron.,* vol. 32, no. 3, pp. 2265–2277, Mar. 2017.

[126] M. K. Bourdoulis and A. T. Alexandridis, "Direct power control of DFIG wind systems based on nonlinear modeling and analysis," *IEEE J. Emerg. Sel. Topics Power Electron.,* vol. 2, no. 4, pp. 764–775, Dec. 2014.

[127] R. Datta and V. T. Ranganathan, "Direct power control of grid-connected wound rotor induction machine without rotor position sensors," *IEEE Trans. Power Electron.,* vol. 16, no. 3, pp. 390–399, May 2001.

[128] L. Xu and P. Cartwright, "Direct active and reactive power control of DFIG for wind energy generation," *IEEE Trans. Energy Convers.,* vol. 21, no. 3, pp. 750–758, Sep. 2006.

[129] J. Hu, J. Zhu, and D. G. Dorrell, "A new control method of cascaded brushless doubly fed induction generators using direct power control," *IEEE Trans. Energy Convers.,* vol. 29, no. 3, pp. 771–779, Sep. 2014.

[130] J. Mohammadi, S. Vaez-Zadeh, S. Afsharnia, and E. Daryabeigi, "A combined vector and direct power control for DFIG-based wind turbines," *IEEE Trans. Sustain. Energy,* vol. 5, no. 3, pp. 767–775, Jul. 2014.

[131] P. Zhou, Y. He, and D. Sun, "Improved direct power control of a DFIG-based wind turbine during network unbalance," *IEEE Trans. Power Electron.,* vol. 24, no. 11, pp. 2465–2474, Nov. 2009.

[132] S. Gao, H. Zhao, Y. Gui, D. Zhou, and F. Blaabjerg, "An improved direct power control for doubly fed induction generator," *IEEE Trans. Power Electron.,* vol. 36, no. 4, pp. 4672–4685, Apr. 2021.

[133] J. Hu, H. Nian, B. Hu, Y. He, and Z. Q. Zhu, "Direct active and reactive power regulation of DFIG using sliding-mode control approach," *IEEE Trans. Energy Convers.,* vol. 25, no. 4, pp. 1028–1039, Dec. 2010.

[134] A. J. Sguarezi Filho and E. R. Filho, "Model-Based predictive control applied to the doubly-fed induction generator direct power control," *IEEE Trans. Sustain. Energy,* vol. 3, no. 3, pp. 398–406, Jul. 2012.

[135] J. Hu, J. Zhu, and D. G. Dorrell, "Predictive direct power control of doubly fed induction generators under unbalanced grid voltage conditions for power quality improvement," *IEEE Trans. Sustain. Energy,* vol. 6, no. 3, pp. 943–950, Jul. 2015.

[136] D. Sun and X. Wang, "Low-complexity model predictive direct power control for DFIG under both balanced and unbalanced grid conditions," *IEEE Trans. Ind. Electron.,* vol. 63, no. 8, pp. 5186–5196, Aug. 2016.

[137] G. Abad, M. Á. RodrÍguez, and J. Poza, "Two-level VSC-based predictive direct power control of the doubly fed induction machine with reduced power ripple at low constant switching frequency," *IEEE Trans. Energy Convers.,* vol. 23, no. 2, pp. 570–580, Jun. 2008.

[138] D. Zhi, L. Xu, and B. W. Williams, "Model-based predictive direct power control of doubly fed induction generators," *IEEE Trans. Power Electron.,* vol. 25, no. 2, pp. 341–351, Feb. 2010.

[139] J. Hu, J. Zhu, Y. Zhang, G. Platt, Q. Ma, and D. G. Dorrell, "Predictive direct virtual torque and power control of doubly fed induction generators for fast and smooth grid synchronization and flexible power regulation," *IEEE Trans. Power Electron.,* vol. 28, no. 7, pp. 3182–3194, Jul. 2013.

[140] Y. Zhang, J. Hu, and J. Zhu, "Three-vectors-based predictive direct power control of the doubly fed induction generator for wind energy applications," *IEEE Trans. Power Electron.,* vol. 29, no. 7, pp. 3485–3500, Jul. 2014.

[141] M. E. Zarei, C. V. Nicolás, J. R. Arribas, and D. Ramírez, "Four-switch three-phase operation of grid-side converter of doubly fed induction generator with three vectors predictive direct power control strategy," *IEEE Trans. Ind. Electron.,* vol. 66, no. 10, pp. 7741–7752, Oct. 2019.

[142] Y. Zhang, J. Jiao, D. Xu, D. Jiang, Z. Wang, and C. Tong, "Model predictive direct power control of doubly fed induction generators under balanced and unbalanced network conditions," *IEEE Trans. Ind. Appl.,* vol. 56, no. 1, pp. 771–786, Jan./Feb. 2020.

[143] M. E. Zarei, C. Veganzones Nicolás, and J. Rodríguez Arribas, "Improved predictive direct power control of doubly fed induction generator during unbalanced grid voltage based on four vectors," *IEEE J. Emerg. Sel. Topics Power Electron.,* vol. 5, no. 2, pp. 695–707, Jun. 2017.

[144] D. Zhi and L. Xu, "Direct power control of DFIG with constant switching frequency and improved transient performance," *IEEE Trans. Energy Convers.,* vol. 22, no. 1, pp. 110–118, Mar. 2007.

[145] N. Amiri, S. M. Madani, T. A. Lipo, and H. A. Zarchi, "An improved direct decoupled power control of doubly fed induction machine without rotor position sensor and with robustness to parameter variation," *IEEE Trans. Energy Convers.,* vol. 27, no. 4, pp. 873–884, Dec. 2012.

[146] R. Sadeghi, S. M. Madani, M. Ataei, M. R. Agha Kashkooli, and S. Ademi, "Super-twisting sliding mode direct power control of a brushless doubly fed induction generator," *IEEE Trans. Ind. Electron.,* vol. 65, no. 11, pp. 9147–9156, Nov. 2018.

[147] P. Xiong and D. Sun, "Backstepping-Based DPC strategy of a wind turbine-driven DFIG under normal and harmonic grid voltage," *IEEE Trans. Power Electron.,* vol. 31, no. 6, pp. 4216–4225, Jun. 2016.

[148] X. Wang, D. Sun, and Z. Q. Zhu, "Resonant-Based backstepping direct power control strategy for DFIG under both balanced and unbalanced grid conditions," *IEEE Trans. Ind. Appl.,* vol. 53, no. 5, pp. 4821–4830, Sep./Oct. 2017.

[149] D. Santos-Martin, J. L. Rodriguez-Amenedo, and S. Arnalte, "Direct power control applied to doubly fed induction generator under unbalanced grid voltage conditions," *IEEE Trans. Power Electron.,* vol. 23, no. 5, pp. 2328–2336, Sep. 2008.

[150] L. Shang and J. Hu, "Sliding-mode-based direct power control of grid-connected wind-turbine-driven doubly fed induction generators under unbalanced grid voltage conditions," *IEEE Trans. Energy Convers.,* vol. 27, no. 2, pp. 362–373, Jun. 2012.

[151] S. Gao, H. Zhao, Y. Gui, D. Zhou, V. Terzija, and F. Blaabjerg, "A novel direct power control for DFIG with parallel compensator under unbalanced grid condition," *IEEE Trans. Ind. Electron.,* to be published.

[152] H. Nian, P. Cheng, and Z. Q. Zhu, "Coordinated direct power control of DFIG system without phase-locked loop under unbalanced grid voltage conditions," *IEEE Trans. Power Electron.,* vol. 31, no. 4, pp. 2905–2918, Apr. 2016.

[153] E. Rezaei, M. Ebrahimi, and A. Tabesh, "Control of DFIG wind power generators in unbalanced microgrids based on instantaneous power theory," *IEEE Trans. Smart Grid,* vol. 8, no. 5, pp. 2278–2286, Sep. 2017.

[154] Y. Zhang, J. Jiao, and D. Xu, "Direct power control of doubly fed induction generator using extended power theory under unbalanced network," *IEEE Trans. Power Electron.,* vol. 34, no. 12, pp. 12024–12037, Dec. 2019.

[155] D. Sun, X. Wang, H. Nian, and Z. Q. Zhu, "A sliding-mode direct power control strategy for DFIG under both balanced and unbalanced grid conditions using extended active power," *IEEE Trans. Power Electron.,* vol. 33, no. 2, pp. 1313–1322, Feb. 2018.
[156] S. Rivera *et al.*, "Multilevel direct power Control—A generalized approach for grid-tied multilevel converter applications," *IEEE Trans. Power Electron.,* vol. 29, no. 10, pp. 5592–5604, Oct. 2014.
[157] G. Abad, M. Á. Rodriguez, and J. Poza, "Three-Level NPC converter-based predictive direct power control of the doubly fed induction machine at low constant switching frequency," *IEEE Trans. Ind. Electron.,* vol. 55, no. 12, pp. 4417–4429, Dec. 2008.
[158] J. Verveckken, F. Silva, D. Barros, and J. Driesen, "Direct power control of series converter of unified power-flow controller with three-level neutral point clamped converter," *IEEE Trans. Power Del.,* vol. 27, no. 4, pp. 1772–1782, Oct. 2012.
[159] R. Portillo, S. Vazquez, J. I. Leon, M. M. Prats, and L. G. Franquelo, "Model based adaptive direct power control for three-level NPC converters," *IEEE Trans. Ind. Inf.,* vol. 9, no. 2, pp. 1148–1157, May 2013.
[160] B. Hu, L. Kang, J. Liu, J. Zeng, S. Wang, and Z. Zhang, "Model predictive direct power control with fixed switching frequency and computational amount reduction," *IEEE J. Emerg. Sel. Topics Power Electron.,* vol. 7, no. 2, pp. 956–966, Jun. 2019.
[161] L. A. Serpa, P. M. Barbosa, P. K. Steimer, and J. W. Kolar, "Five-level virtual-flux direct power control for the active neutral-point clamped multilevel inverter," in *Proc. IEEE Power Electron. Spec. Conf.*, Jun. 15–19, 2008, pp. 1668–1674.
[162] S. Ouchen, M. Benbouzid, F. Blaabjerg, A. Betka, and H. Steinhart, "Direct power control of shunt active power filter using space vector modulation based on super twisting sliding mode control," *IEEE J. Emerg. Sel. Topics Power Electron.,* to be published.
[163] Y. Liu, B. Ge, H. Abu-Rub, H. Sun, F. Z. Peng, and Y. Xue, "Model predictive direct power control for active power decoupled single-phase Quasi-Z -Source inverter," *IEEE Trans. Ind. Inf.,* vol. 12, no. 4, pp. 1550–1559, Aug. 2016.
[164] W. Song, Z. Deng, S. Wang, and X. Feng, "A simple model predictive power control strategy for single-phase PWM converters with modulation function optimization," *IEEE Trans. Power Electron.,* vol. 31, no. 7, pp. 5279–5289, Jul. 2016.
[165] Z. Liu, C. Xiang, Y. Wang, Y. Liao, and G. Zhang, "A model-based predictive direct power control for traction line-side converter in high-speed railway," *IEEE Trans. Ind. Appl.*, vol. 53, no. 5, pp. 4934–4943, Sep./Oct. 2017.

Shuo Yan (Member, IEEE) received the B.Eng. degree from the University of South China, Heng'yang, China, in 2007, the M.Eng. degree from Southeast University, Nanjing, China, in 2010, and the Ph.D. degree with The University of Hong Kong, Hong Kong, in 2016, all in electrical engineering.

He was a Postdoctoral Fellow in power electronics and control with The University of Hong Kong, from 2016 to 2019. He is currently a Senior Lecturer with RMIT University, Melbourne, VIC, Australia. His current research interests include power electronics and control, smart grids, and renewable energy.

Yongheng Yang (Senior Member, IEEE) received the B.Eng. degree in electrical engineering and automation from Northwestern Polytechnical University, Xian, China, in 2009, and the Ph.D. degree in energy technology from Aalborg University, Aalborg, Denmark, in 2014.

He was a postgraduate student with Southeast University, China, from 2009 to 2011. In 2013, he spent three months as a Visiting Scholar with Texas A&M University, USA. Since 2014, he has been with the Department of Energy Technology, Aalborg University, where he became a tenured Associate Professor in 2018. In January 2021, he joined Zhejiang University, Hangzhou, China, where he is now a ZJU100 Young Professor with the Department of Electrical Engineering. His current research is to tackle the issues brought by the integration of photovoltaic systems and multienergy vectors through developing reliable and efficient power converters with advanced control.

Dr. Yang was the Chair of the IEEE Denmark Section (2019–2020). He is the Secretary for the Technical Committee of Sustainable Energy Systems of the IEEE PELS. He is an Associate Editor for several IEEE transactions/journals and a Deputy Editor for the *IET Renewable Power Generation for Solar Photovoltaic Systems*. He received the 2018 *IET Renewable Power Generation* Premium Award and was an Outstanding Reviewer for the IEEE TRANSACTIONS ON POWER ELECTRONICS in 2018. In addition, he has received two IEEE Best Paper Awards.

S. Y. (Ron) Hui (Fellow, IEEE) received the B.Eng. (hons.) degree in electrical and electronic engineering from the University of Birmingham, Birmingham, U.K., in 1984, and the D.I.C. and Ph.D. degrees in electrical engineering from Imperial College London, London, U.K., in 1987.

Previously, he held academic positions with the University of Nottingham and the University of Sydney. During 2011–2021, he was the Philip Wong Wilson Wong Chair Professor at the University of Hong Kong. Presently, he holds the MediaTek Endowed Professorship with Nanyang Technological University, Singapore, and a Chair Professorship with Imperial College London, London, U.K. He has authored or coauthored more than 450 research papers including 300 refereed journal publications. More than 60 of his patents have been adopted by industry worldwide. His research interests include power electronics, wireless power, sustainable lighting, and smart grid. His inventions on wireless charging platform technology underpin key dimensions of Qi, the world's first wireless power standard, with freedom of positioning and localized charging features for wireless charging of consumer electronics. He also developed the Photoelectrothermal Theory for LED Systems.

Dr. Hui was a recipient of the IEEE Rudolf Chope R&D Award and the IET Achievement Medal (The Crompton Medal) in 2010, and the IEEE William E. Newell Power Electronics Award in 2015. He is a fellow of the Australian Academy of Technology and Engineering, U.S. National Academy of Inventors, and Royal Academy of Engineering, U.K.

Frede Blaabjerg (Fellow, IEEE) received the Ph.D. degree in electrical engineering from Aalborg University, Aalborg, Denmark, in 1995.

He was with ABB-Scandia, Randers, Denmark, from 1987 to 1988. He became an Assistant Professor in 1992, an Associate Professor in 1996, and a Full Professor of power electronics and drives in 1998. In 2017, he became a Villum Investigator. He is an honoris causa at University Politehnica Timisoara, Timisoara, Romania, and Tallinn Technical University, Tallinn, Estonia. His current research interests include power electronics and its applications such as in wind turbines, PV systems, reliability, harmonics, and adjustable speed drives. He has authored or coauthored more than 600 journal papers in the fields of power electronics and its applications. He is the co-author of four monographs and editor of ten books in power electronics and its applications.

Dr. Blaabjerg was a recipient of 33 IEEE Prize Paper Awards, the IEEE PELS Distinguished Service Award in 2009, the EPE-PEMC Council Award in 2010, the IEEE William E. Newell Power Electronics Award 2014, the Villum Kann Rasmussen Research Award 2014, the Global Energy Prize in 2019, and the 2020 IEEE Edison Medal. He was the Editor-in-Chief for the IEEE TRANSACTIONS ON POWER ELECTRONICS from 2006 to 2012. He was a Distinguished Lecturer for the IEEE Power Electronics Society from 2005 to 2007 and for the IEEE Industry Applications Society from 2010 to 2011 as well as from 2017 to 2018. During 2019–2020, he served as the President of the IEEE Power Electronics Society. He has been the Vice President of the Danish Academy of Technical Sciences. He was nominated in 2014–2020 by Thomson Reuters to be among the 250 most-cited researchers in engineering in the world.